The effect of support morphology on the performance of Co/CeO_2 catalysts for ethanol steam reforming

---

A Bachelors of Science Thesis

Prepared in Accordance to Requirements for:

Graduation with Honors in Engineering

And

Graduation with Distinction in Chemical and Biomolecular Engineering

Written By: Hyun Tae Sohn

The Ohio State University 2011

Thesis Committee:

Dr. Umit S. Ozkan, Advisor

Dr. David Tomasko

Copyright by

Hyun Tae Sohn

2011

Abstract

Hydrogen is considered a major candidate for future energy carriers. However, the typical methods of producing hydrogen such as gasoline and natural gas reforming are not environmentally clean. Bio Ethanol steam reforming (BESR) which is a carbon-emission free process shows potential for production of hydrogen. Cobalt based catalysts have shown promising BESR activity and are economically viable alternatives to the traditional noble metal based (Ni, Rh, Pt). Cerium oxide based supports are shown to have higher oxygen mobility which enhances catalyst activity. A more detailed research of the different morphologies of CeO_2 nanocrystals such as polyhedra, rods and cubes can improve our understanding of the effect of support morphology on BESR. Therefore, in this paper the catalytic performance of cobalt catalysts supported on CeO_2 in different morphologies was investigated for production of hydrogen via BESR. The cobalt-based catalysts were synthesized by precipitation and hydrothermal method and prepared by incipient wetness impregnation (IWI). Those catalysts were characterized through various techniques such as transmission electron microscopy (TEM), Brunauer-Emmett-Teller (BET) surface area measurements as well as steady-state activity testing on catalyst performance with a gas chromatograph (GC). With the current data provided by the GC, Co/CeO_2 nanocubes showed the best catalytic performance at high temperature (450, 500 ℃), indicating the highest hydrogen yield of 96 % and 100% ethanol conversion at 500 ℃. Also, Co/CeO_2 nanopolyhedra were the most active catalysts at low temperature (350, 400 ℃), having the highest hydrogen yield of 87.5% and 93.5% ethanol conversion at 400 ℃. Therefore, it is concluded that the effects of different actives sites and crystal planes of support morphologies play a role in improving the catalytic performance of Co/CeO_2 for BESR.

Dedication

Dedicated to My Parents

Acknowledgements

First and foremost, my utmost gratitude to Dr. Umit S. Ozkan, a professor in Chemical and Biomolecular Engineering Department, who provides me the opportunity to work in her Heterogeneous Catalyst Research Group (HCRG) as an undergraduate research assistant. This honors thesis could have not been possible without her continuous guidance and encouragement. The experiences and knowledge that I have gained in the past two years in her laboratories not only have greatly improved my personal skills in chemical engineering but also have become the foundation for pursuing a PhD degree in our department. I am fortunate to have had Dr. Ozkan as an advisor and mentor and could not even imagined a better undergraduate advisor than her.

I would like to thank Ibrahim Ilgaz Soykal who spent most of the time with me working on the bio ethanol steam reforming project. His enthusiasm and insight in this research have had always motivated me. From Ilgaz, I have learned everything about this project from the most basics to the most expert knowledge. I truly thank of his time, effort, and advice that significantly helped me write this paper and have a better understanding for our project.

I would like to show my sincere gratitude to all the members of Dr.Ozkan's Heterogeneous Catalyst Research Group (HCRG) for sharing their instruments and numerous stimulating discussions that we have had in the group meetings as well as in laboratories. I also appreciate for creating a good atmosphere to enable all the lab fellows to focus on their projects.

Finally, I would like to thank my parents for their constant support: financially, emotionally and mentally. I have been always grateful to my dad for helping me study abroad and pursue my future career. I do not know how to express the gratitude for my mom in words, who has dedicated her whole life for me. I am thankful to her for encouraging me to become a better person and for helping me live a successful life.

Table of Contents

List of Figures

List of Tables

List of Equations

Nomenclature

General

BESR	Bio Ethanol Steam Reforming
BET	Brunauer, Emmett and Teller
FID	Flame Ionization Detector
GC	Gas Chromatograph
PDHID	Pulsed Discharge Helium Ionization Detector
TEM	Transmission Electron Microscopy

Chemicals

CeO_2	Cerium Oxide
Co	Cobalt
H_2	Hydrogen
H_2O	Water
CH_4	Methane
C_2H_5	Ethane
CH_3CHO	Acetaldehyde
CO	Carbon Monoxide
CO_2	Carbon Dioxide
C_3H_7	Propane
$(CH_3)_2CO$	Acetone
$(C_2H_5)_2O$	Di-Ethylether
C_2H_5OH	Ethanol

Calculations

$\dot{\mathbf{N}} = \text{Molar Flow Rate of Hydrogen } (\frac{\text{mol}}{\text{min}})$

$\dot{\mathbf{V}} = \text{Volumetric Flow Rate of Hydrogen } (\frac{\text{ml}}{\text{min}})$

$\boldsymbol{\rho}\ \left(\frac{\text{kg}}{\text{m}^3}\right) = \text{Density} \qquad \mathbf{M}\ \left(\frac{\text{mol}}{\text{gmol}}\right) = \text{Molecular Weight}$

$\mathbf{P} = \text{Pressure} \quad \mathbf{T} = \text{Temperature}$

$\mathbf{R}\ (\text{Gas Constant}) = 8.205746 \times 10^{-5}\ (\frac{\text{m}^3 \cdot \text{atm}}{\text{K} \cdot \text{mol}})$

1. Introduction

Increase in the price of fossil fuel and depletion of the reserves have been an indication of the need to research alternative and renewable energy sources. Besides, the increasing environmental pollution also establish grounds for studying green production processes of those energy sources. These new energy demands could be met by hydrogen which has been widely accepted as an efficient energy carrier for the next generation [1]. The reasons are that hydrogen is the most abundant gas in the world, and does not generate any greenhouse gases throughout combustion process [1, 2]. Also, hydrogen has relatively high energy storage capacity on a mass basis than other fuels such as methane, gasoline and coal [1]. Therefore, hydrogen has been emphasized and investigated in many articles regarding production techniques, applications and its economical feasibility [3-5].

The typically way to produce hydrogen is known as either gasoline or natural gas reforming in the United States. From the literature review, 95% of hydrogen production in United States is based on steam reforming and approximately 50% of hydrogen produced in worldwide uses natural gas reforming [6]. Since gasoline and natural gas reforming are not environmental friendly, there have been extensive studies in finding various feedstocks for producing hydrogen. Among different materials such as methanol, ethanol, dimethlyether and methane [7-10], alcohol steam reforming can be performed at relatively low temperature obtaining higher hydrogen yield [11]. For those reasons, especially ethanol which is non-toxicity and high hydrogen contents has been focused recently in the stream reforming field.

Instead of using ethanol directly as a reactant in hydrogen production process, the usage of bio-derived liquids such as bio-ethanol can be environmentally cleaner and more cost competitive. Bio-ethanol can be obtained though hydrolysis and fermentation from non-grain

plant materials such as corn stover which is the most abundant growing crop in United States. From the U.S. Department of Agriculture at 2002, the average total area for corn was roughly 31.9 % of the total planting area in United States [12]. This result indicates that the potential availability of bio-ethanol to steam reforming is plentiful; hence, it can be a practical application in industry. Moreover, bio-ethanol steam reforming is theoretically carbon-emission free process since carbon dioxide is the only gas emitted throughout the reaction. Carbon dioxide is considered as greenhouse gas in common; however, the emitted carbon dioxide gas from bio-ethanol steam reforming can be reusable to the plants through photosynthesis [2].

The overall reaction for bio-ethanol stream reforming is shown as follows [2]:

$$C_2H_5OH(l) + 3H_2O(l) \longrightarrow 6H_2(g) + 2CO_2(g) \qquad [1.1]$$

$$\Delta H = 348 \text{ kJ/mol at } 25℃$$

Under constant pressure and temperature the reaction is endothermic thus the BESR system adsorbs heat from the surrounding. Also, one mole of ethanol can theoretically produce 6 moles of hydrogen. However, in practically, lots of byproducts can be observed through complex reaction mechanisms. Side reactions and its resulted products from BESR can be seen in the following equations [2]:

$C_2H_5OH(l) \longrightarrow CH_4(g) + CO(g) + H_2(g)$	(Ethanol Decomposition)	[1.2]
$C_2H_5OH(l) \longrightarrow CH_3CHO(g) + H_2(g)$	(Dehydrogenation)	[1.3]
$C_2H_5OH(l) \longrightarrow C_2H_4(g) + H_2O(l)$	(Dehydration)	[1.4]
$C_2H_5OH(l) + H_2O(l) \longrightarrow 2CO(g) + 4H_2(g)$	(Incomplete Reforming)	[1.5]
$2C_2H_5OH(l) \longrightarrow (C_2H_5)_2O(g) + H_2O(l)$	(Dehydrative Coupling)	[1.6]
$CO(g) + 3H_2(g) \longrightarrow CH_4(g) + H_2O(l)$	(Methanation)	[1.7]

Lots of intermediate byproducts such as methane, ethane, acetaldehyde, diethyl ether, and carbon monoxide are obtained through side reactions. However, hydrogen can be also achieved from ethanol decomposition, dehydrogenation and incomplete reforming. Therefore, it is very important to remove undesired byproducts in order to maximize the hydrogen production. One possible method to eliminate intermediate byproducts is the C-C bond cleavage which can be done by using catalysts [13]. Therefore, diverse catalysts have been extensively studied.

Auprêtre et al. [14] have carried out the bio ethanol steam reforming on noble-metal catalysts such as Ni, Rh, Pt, Cu, Zn and Fe over several of supports. They conclude that from those supported metal catalysts hydrogen and carbon dioxide production is dominant in BESR. This result shows that metal catalysts are believed to have good catalytic activity which improves hydrogen production in BESR. Another paper from Llorca et al. [15] first proposed that metallic cobalt-based catalysts are very efficient for ethanol steam reforming. By using 1% cobalt loaded catalysts, they obtained a hydrogen selectivity of 73.8 % and 100% ethanol conversion. The authors concluded that cobalt containing catalysts show a high activity for BESR. Literature suggests that cobalt supported catalysts show promising performance on bioethanol steam reforming [6, 16, 17].

The supporting materials are also very important for catalyst activity. The interactions between catalyst precursor and the support are found to have a significant effect on the overall performance. For example, the oxygen mobility of the support has been investigated by Hua et al. [18] and for cobalt based catalyst over ZrO_2 and CeO_2. The results show that the cerium oxide which has high oxygen storage capacity has higher catalytic activity than ZrO_2. Therefore, in this study Co/CeO_2 was used as catalyst on bioethanol steam reforming.

Although there has been many studies exploring characteristics of Co/CeO_2 and techniques to improve the catalytic activity of Co/CeO_2 [19-21], the effect of CeO_2 morphology on the performance of Co/CeO_2 has not been focused. Recent studies indicate that CeO_2 nanopolyhedra, nanorods and nanocubes have different actives sites and crystal planes that show different catalytic activities. Haiso et al. have been reported that CeO_2 nanorods resulted in good hydrogen selectivity than nanopolyhedra in ethanol steam reforming [22]. Zhou et al. found that CeO_2 nanorods are better catalysts than nanopolyhedra for CO oxidation [23].

In the present work, we have examined the impact of CeO_2 morphology on the Co/CeO_2 catalytic performance on bioethanol steam reforming. The CeO_2 nanopolyhedra, nanorods and nanocubes were synthesized by precipitation and hydrothermal methods. Cobalt precursor was then impregnated to the support by incipient wetness impregnation (IWI). The CeO_2 morphologies were imaged by transmission electron microscope (TEM) and Brunauer-Emmett-Teller (BET) surface area and porosity analysis was conducted as characterization techniques. The catalysts activity tests were performed in a specifically designed BESR system and all the results were used to compare the catalytic activity deviations from Co/CeO_2 morphologies.

2. Experimental

2.1 Catalyst Preparation

A. Synthesis of CeO_2 Support Morphology

- Nanopolyhedra

First Stage: *$Ce(NO_3)_3 \cdot 6H_2O$ (1.5 g, 99.9%) was dissolved in water (9.4 ml), and then excess NaOH solution (11 wt.%) was added. It was stirred for 15min under room temperature.*

Among diverse techniques that were studied to synthesize CeO_2 nanopolyhedra, the precipitation method was chosen because of its simplicity in the process and lower production cost compared to other techniques. In addition, the precipitation technique allows the experimenter to easily scale-up when larger amount of product is needed. In here, the insoluble solids (precipitate) which are formed from the reaction between positive ions (cations) and negative ions (anions) in the solution, was obtained as the intermediate product. The cerium nitrate in the aqueous phase was used to provide cations (Ce^{3+}) as well as the sodium hydroxide in the aqueous phase was used to offer anions (OH^-). The overall reaction can be described as follows.

$$Ce(NO_3)_3\,(aq) + 3\ NaOH\ (aq) \rightarrow Ce(OH)_3\,(s) + 3\ NaNO_3\,(aq) \qquad [2.1.1]$$

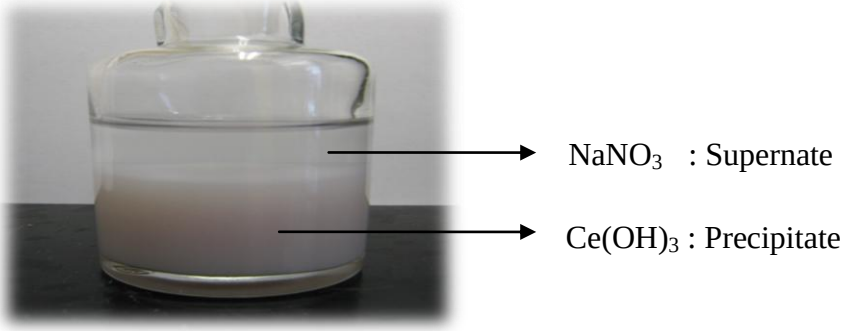

Figure 2.1.1 Precipitation Method

The purple slurry which can be seen in Figure 2.1.1 indicates $Ce(OH)_3$ as precipitate [22]. The remaining liquid $NaNO_3$ is called supernate which was filtered in the next stage.

Second Stage: *The suspension was filtered, and the remaining solids at the top were rinsed with deionized water (1.5 L) until the pH value of around 7 is reached. Then, the obtained solid products were dried under room temperature for one day.*

The pH value of the suspension was increased to 12 after excess NaOH was added in the first stage. Thus, washing step was conducted in order to reduce the basicity of the filtered solids.

Third Stage: *The dried $Ce(OH)_3$ nanopolyhedra were calcined at 450 ℃ for 3 h in air at 10℃ ramp rate.*

The acquired intermediate product from the second stage were $Ce(OH)_3$ nanopolyhedra. To remove the impurities and create the support matrix, the dried solids were calcined. After the calcinations process, CeO_2 nanopolyhedra were obtained as light yellow product at the end.

- Nanorods

First Stage: *$Ce(NO_3)_3 \cdot 6H_2O$ (1.5 g, 99.9%) was dissolved in water (9.4 ml), and then excess NaOH solution (11 wt.%) was added. It was stirred for 15min under room temperature.*

The first step of the procedure of synthesizing CeO_2 nanorods and nanocubes is basically the same as explained in the previous section regarding nanopolyhedra. However, after mixing, the suspension was transferred into a stainless-steel vessel and maintained for one day under autogeneous pressure and high temperature to crystallize in rods and cubes.

Second Stage: *The suspension was transferred to an autoclave, was heated at 110 ℃ for 24 hours in the oven.*

The process is called “hydrothermal synthesis”. The hydrothermal method has the meaning of any heterogeneous reactions in aqueous solutions under high pressure and temperature conditions in a closed system. The method is applicable for the synthetic routes for nanocrystal morphology preparation under specific applications. The high pressure and temperature stimulates the crystal growth of the insoluble solids that are precipitated in the solution in a certain way and forms various shapes. The hydrothermal method has the merit of low production cost for oxide mixtures because the structure of complex oxide morphologies can be formed immediately after reaction. [24]. In order to create the hydrothermal conditions, a pressure vessel which is known as ‘autoclave’ is required to capture the heat and high pressure. There are many existing autoclaves those which hold different pressures and temperatures.

Table 2.1.1 Different Types of Autoclaves [24]

Type	Characteristic Data
Pyrex tube 5 mm i.d. 2mm wall thickness	**6 bar at 250 ℃**
Quartz tube 5mm i.d. 2mm wall thickness	**6 bar at 300 ℃**
Flat plate seal, Morey type	**400 bar at 400 ℃**
Welded Walker-Buehler closure 2600 bar at 350C	**2 kbar at 480 ℃**
Delta ring, unsupported area	**2.3 kabr at 400 ℃**
Modified Bridgman, unsupported area	**3.7 kbar at 500 ℃**
Full Bridgman, unsupported area	**3.7 kbar at 750 ℃**
Cold-cone seal, Tuttle-Roy type	**5 kbar at 750 ℃**
Piston cylinder	**40 kbar, 1000 ℃**
Belt apparatus	**100kbar, >1500 ℃**
Opposed anvil	**200 kbar, >1500 ℃**
Opposed diamond anvil	**up to 500 kbar, >2000 ℃**

Not only the autoclave itself is needed, but also a proper lining or separate liners for the inner wall of the autoclave are necessary for high purity of crystals. Generally, Teflon is an appropriate lining to contain for hydroxides and chlorides solutions. Therefore, in the experiment, an autoclave with stainless steel shell and Teflon vessel was used. This autoclave was designed recently and it is not listed in Table 2.1.1. The autoclave was able to be heated up to 250 ℃ and was able to withstand the pressure of 40 bars.

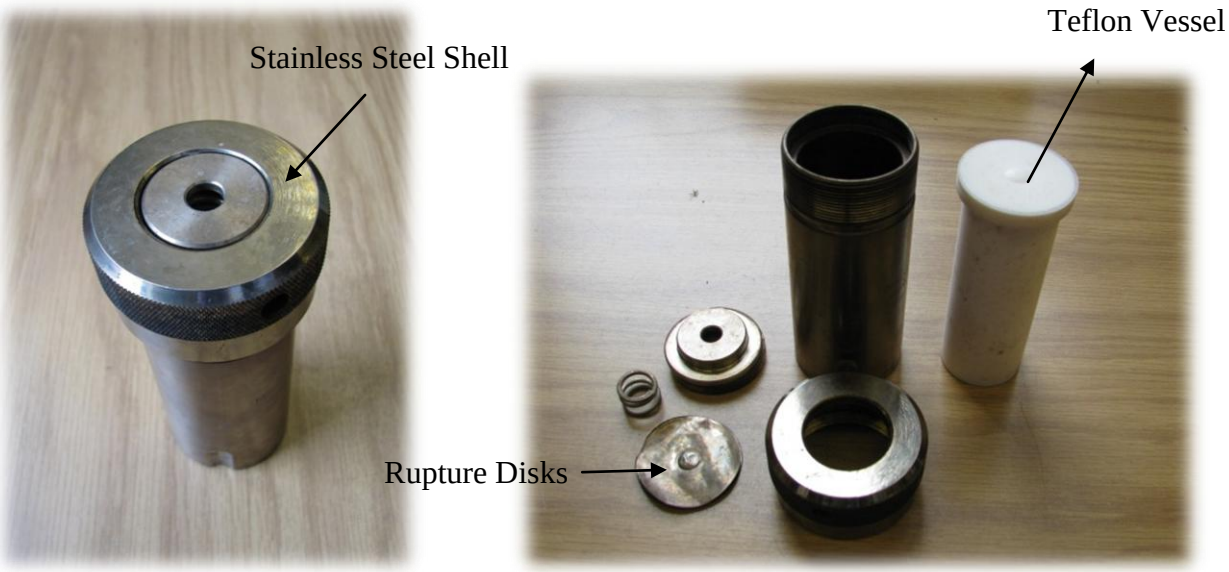

Figure 2.1.2 Small Size Autoclave

Third Stage: *The autoclave was cooled to room temperature. The suspension was filtered, and the remaining solids were rinsed with deionized and distilled water (1.5 L) until the pH value was reached around 7. Then, the solids were dried under room temperature for one day. The dried* $Ce(OH)_3$ *nanorods were calcined at 450 ℃ for 3 h in air to yield* CeO_2 *nanorods as light yellow product.*

The procedures after hydrothermal process are identical to the procedures for nanopolyhedra. $Ce(OH)_3$ rods were calcined to constitute the crystal structure of CeO_2 nanorods.

- Nanocubes

All the experimental procedures for nanocubes basically follow the exact same way of the nanorods synthetic method. The only difference was that the autoclave was heated at 200 ℃, whereas nanorods were 110 ℃.

First Stage: *$Ce(NO_3)_3 \cdot 6H_2O$ (1.5 g, 99.9%) was dissolved in water (9.4 ml), and then excess NaOH solution (11 wt.%) was added. It was stirred for 15min under room temperature.*

Second Stage: *The suspension was transferred to an autoclave, was heated at* ***200 ℃*** *for 24 hours in the oven.*

Third Stage: *The autoclave was cooled to room temperature. The suspension was filtered, and the remained solids were rinsed with deionized water (1.5 L) until the pH value was reached around 7. Then, the solids were dried under room temperature for one day. The dried $Ce(OH)_3$ nanocubes were calcined at 450 ℃ for 3 h in air to yield CeO_2 nanocubes as light yellow product.*

- Color Changes of CeO_2 Support Morphologies

The importance of the color change of supports was not magnified in studies and was negligible. This is because the degree of the color change of the support was indeterminacy. In other words, the degree of the color change seen by the experimenters vary from person to person, thus it can be obscure in the scientific point of view. However, the color change of supports that were occurred throughout the experiment process was significantly helpful in the

determination of CeO_2 morphologies and confirming that the nanocrystals were actually formed. Figure 2.1.3 shows a detailed color change of supports in a sequential order.

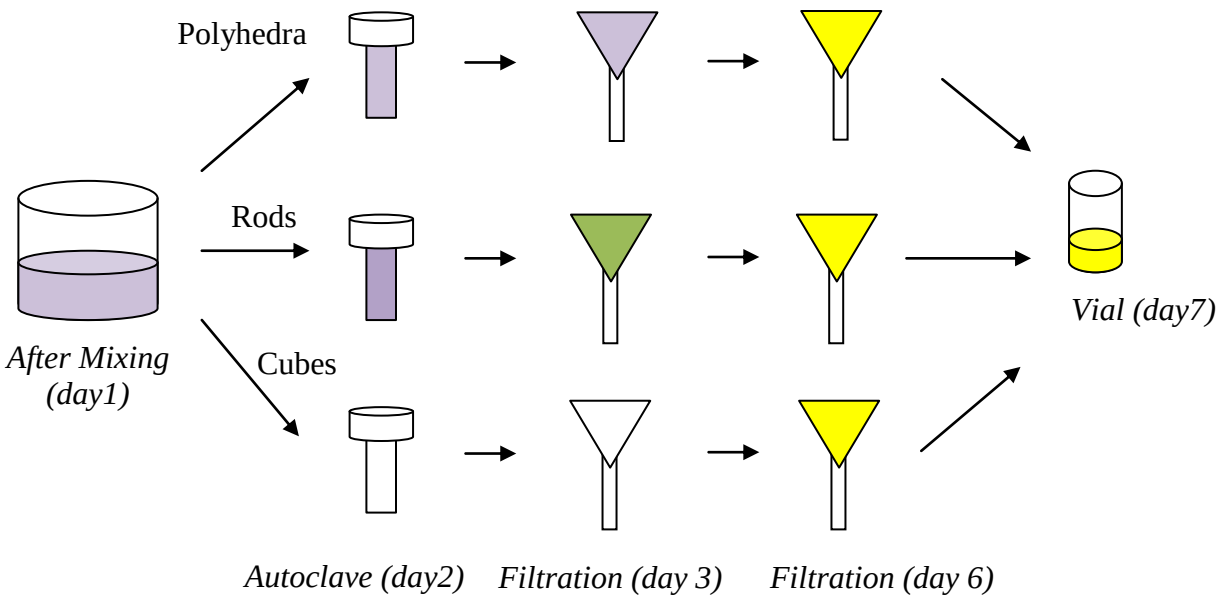

Figure 2.1.3 Color Change of CeO_2 Support Morphologies

B. Cobalt Impregnation on CeO_2 Support Morphology

Sigma-Aldrich-Cobalt (II) nitrate hexahydrate (98%) was used as the cobalt precursor, and was dissolved in ethanol. The solution was impregnated on the prepared CeO_2 support and it was dried at 95 ℃ for overnight, calcined at 450 ℃ for 3 h in air to obtain 10% weight loading Co/CeO_2.

The incipient wetness impregnation (IWI) method is widely used for catalysts synthesis especially in the case that the metal precursor is incorporated with the support. In here, the ethanol solution which contains cobalt precursor was added on the support in several drops

(±0.30 ml, pore volume of the support) and then mixed by a glass rod in order to dissipate the cobalt solution on the surface equally. After drying for overnight, it was repeated as needed. The sample calculations of 10% wt. cobalt loading are can be seen below.

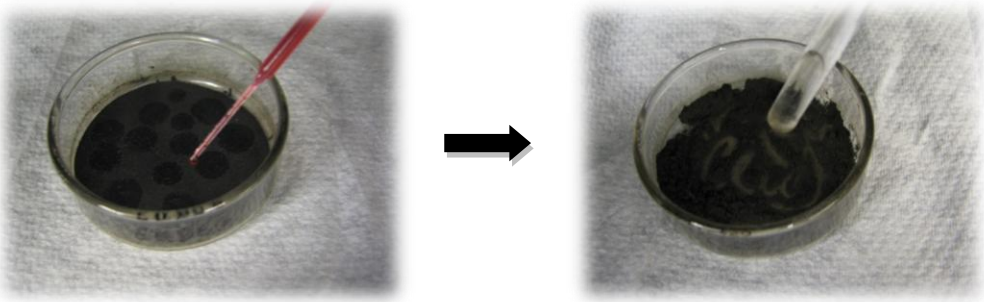

Figure 2.1.4 Cobalt Incipient Wetness Impregnation (IWI)

The catalytic performance of the supported cobalt catalysts substantially depends on this cobalt dispersion on the support. A paper reported that the 10% weight loading Co/CeO_2 catalysts synthesized by incipient wetness impregnation (IWI) technique resulted in higher hydrogen yields in steady-state reaction than other techniques. Their characterization results indicate that the oxygenated carbonaceous were remained on the surface of the CeO_2 support after cobalt IWI, which can preserve the cobalt dispersion in the BESR reaction and obstruct side reactions [21].

- Sample Calculation for Cobalt loading:

2g of CeO_2 support ⟶ 10% weight loading Co/CeO_2

$$\frac{mass\ of\ cobalt}{2 + mass\ of\ coblt} \times 100 = 10\ \% \quad \rightarrow \quad mass\ of\ cobalt = 0.22\ g$$

$$moles\ of\ cobalt = \frac{0.22}{58.33\ (= Cobalt\ Molecular\ Weight)}\ g = 0.0038\ mol$$

$$0.0038\ \times 291.03\ \left(= Molecular\ Weight\ of\ Co(NO_3)\right) = \mathbf{1.1\ g\ of\ Co(NO_3)\ needed}$$

2.2 Catalyst Characterization

A. Transmission Electron Microscope (TEM)

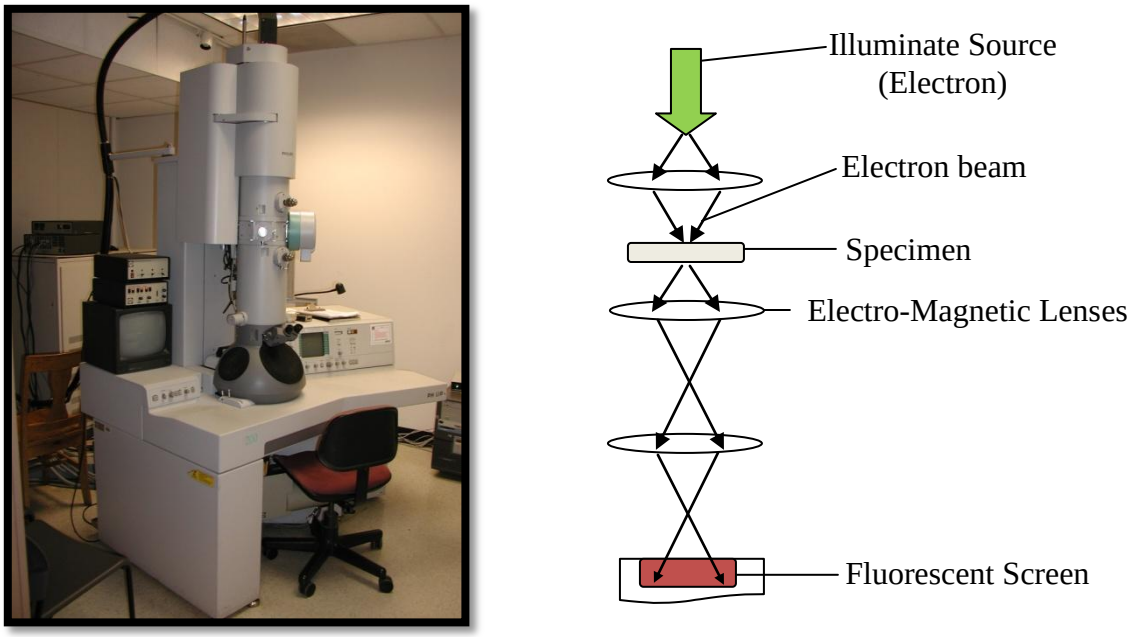

Figure 2.2.1 TEM and the Basic Principle [26, 27]

TEM images for the prepared CeO_2 morphologies were taken by using CM-200 operated at 200 kV. This TEM instrument shows a 2.7 Å resolution using twin lens with ±70° sample tilt and ±45° on 2nd tilt [26]. Because of the access difficulties with the instrument as an undergraduate student, the images were taken by one of the PhD students in the lab (Ibrahim Ilgaz Soykal).

The transmission electron microscope shares similar function principle with light microscope. However, for TEM, electron is used as the illuminate source. According to this difference, TEM images show much higher resolutions than light microscope. The wavelength of accelerated electrons can go as low as 6 pm compared to 500 nm wavelength for a typical light microscope [27]. The magnification of the microscope can be enhanced significantly at lower wavelength, hence using TEM instrument nanosized materials can be photographed. The basic

principle of TEM is shown in Figure 2.2.1. The electrons are first emitted at the top where the illuminate source is located. After those electrons are gathered by the electro-magnetic lense, it generates a very thin electron beam. The electron beam then penetrates the specimen and some of the electrons are dispersed or vanish from the electron beam by hitting the sample. The evaded electrons reach to the fluorescent screen on the bottom and develop the bright part of the image. Therefore, the density of the specimen has an immense effect on the formation of the TEM images [27].

B. BET Surface Area and Porosity Analysis

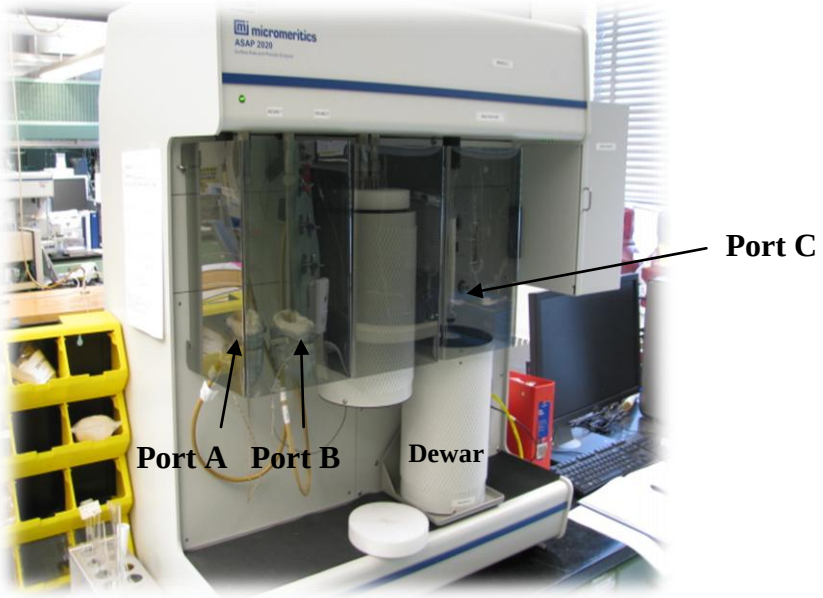

Figure 2.2.2 ASAP 2020 – Micromeritics

Both Co/CeO_2 catalysts and CeO_2 supports were first degassed with nitrogen for 12 h under 130 °C. Then, those were analyzed in generic run microporous samp condition. The BET surface area and pore volume were collected.

BET surface area analysis technique was first proposed by three people whose names are Stephen Brunauer, Paul Hugh Emmett and Edward Teller in 1938. The term BET comes from the first initials of their last names. They presented the BET theory which can be used for the measurement of catalyst surface area and porosity though physical and chemical adsorption of gas molecules on a catalyst surface [28]. Physical adsorption happens when the adsorptive molecules adhere to the catalyst surface through Van der Waals force, whereas chemical adsorption forms a chemical bond on the interface. This difference causes a deviation of technical limitations for physical and chemical adsorption. One of the most significant characteristic is that physical adsorption is optimized at very low temperature whereas chemical adsorption can be applied in a wide range of temperature. In this experiment, BET analysis using physical adsorption was conducted, therefore a white dewar was filled with liquid nitrogen during physical adsorption which allowed a complete adsorption and desorption by maintained a very low temperature.

Among many BET surface area and porosity analyzers, ASAP 2020 from micromeritics which is shown in Figure 2.2.2 was used. Prior to the analysis, the catalysts were first degassed to clean the surface under vacuum. Two degas ports (A, B) are located on the left side. The heating mantles with thermocouple at the bottom were used to sustain the temperature at 130 ℃. After degassing was completed, the sample tube was transferred to the right port (C) for the analysis and nitrogen was used as absorptive gas. The surface area and pore volume was generated to screen either graphically or numerically.

2.3 Catalytic Activity Test

A. The Design of BESR Reactor System

The catalytic activity test for supported cobalt catalysts was performed in a BESR reactor system that has been previously designed by Hua Song, Lingzhi Zhang, Rick B. Watson, Drew Braden, Ibrahim Ilgaz Soykal and Dr. Umit S. Ozkan at The Ohio State University, Heterogeneous Catalysis Research Group in Chemical Engineering Department. The shown Figure 2.3.2 is a simplified version of their schematic diagram of the reactor system for BESR. Only the lines and components that are related to sample pretreatment and reaction steps are portrayed.

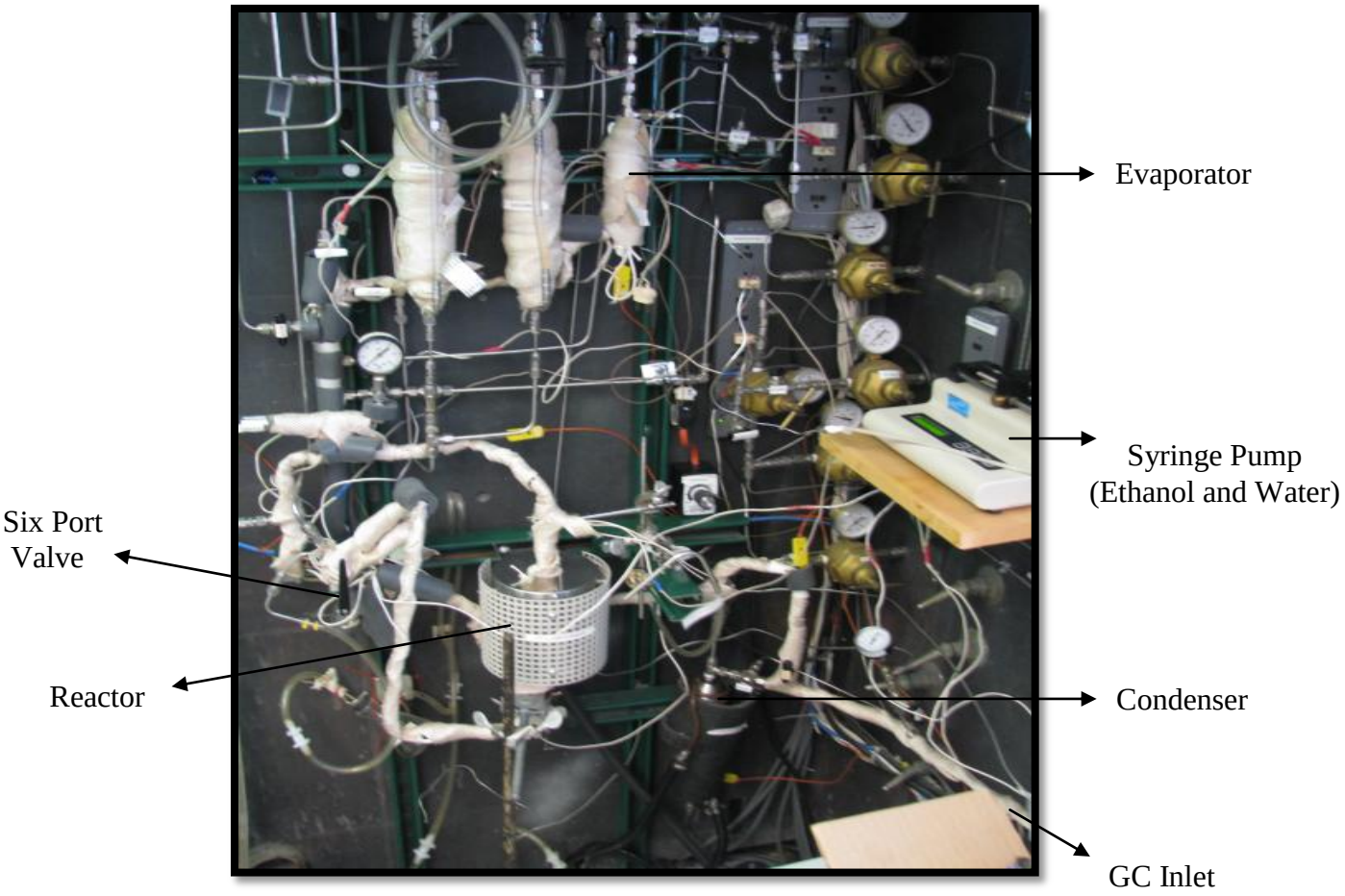

Figure 2.3.1 The Reactor System for BESR

Figure 2.3.2 Simplified Diagram of the Reactor System

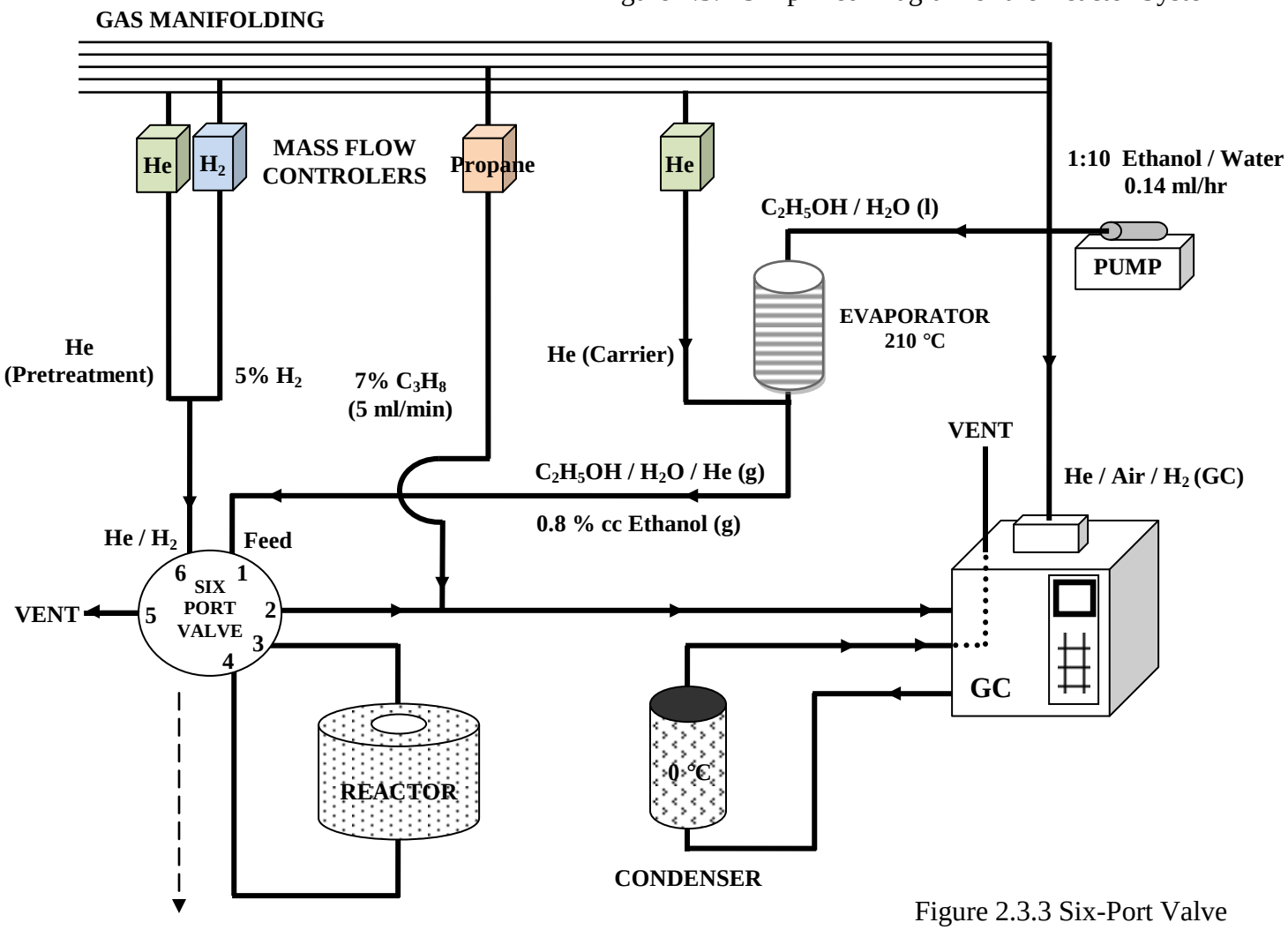

Figure 2.3.3 Six-Port Valve

● How six port valve works for each step

- Pretreatment / Feed Analysis

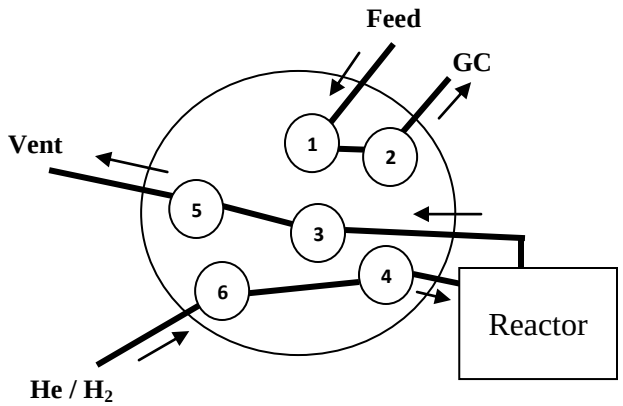

Feed→ 1 → 2 → GC

Pretreatment Gas (He/H_2) → 6 → 4 → React → 3 → 5 → Vent

- Reaction

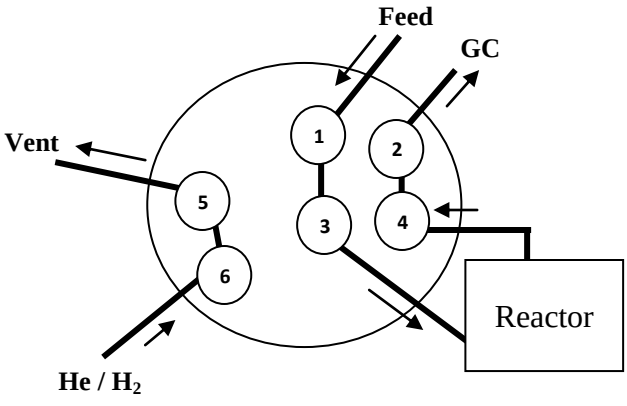

Feed→ 1 → 3 → React → 4 → 2 → GC

Pretreatment Gas (He/H_2) → 6 → 5 → Vent

The reactant liquid is synthesized by mixing ethanol and water at 1:10 molar ratio. The composition of the reactant is determined from the composition of bio-ethanol stream by biomass fermentation. The reactant is then delivered by a syringe pump to the evaporator which is held at 210 ℃. The water and ethanol is assumed to be evaporated completely so that the composition of 1:10 molar ratio is maintained through evaporation. The feed stream after evaporator consists of gas phase reactants, and helium is added as carrier gas. The feed stream is then moved to six port valve. The concentration of the feed stream is aimed at 0.8% ethanol in total volumetric flow rate of 30 ml/min. To obtain this fraction, the input volumetric flow rate of the 1:10 molar ratio ethanol/water solution is calculated as 0.14 ml/hr. A detailed calculation for estimating the input volumetric flow rate is located at Appendix A. The Pretreatment stream line is also introduced to the six port valve as well, and it is comprised of 5% hydrogen and helium gas. All the volumetric flow rates are managed by the mass flow controllers at the top. The sample pretreatment and reaction can be run at the same time with this system by using the six port valve. When it was set for sample pretreatment step, the feed line is directly connected to the gas chromatography bypassing the reactor and the pretreatment line is coupled to the reactor. This allows performing feed analysis and sample pretreatment simultaneously. When the six port valve is adjusted for reaction step, the pretreatment line is linked to the vent and the feed line is connected to the reactor. The product stream from the reactor is sent to a gas chromatography for the catalytic performance analysis. The 7% propane gas of 5 ml/min is then added as internal standard. After the product stream is analyzed by the first detector in the GC (FID), it is brought to the condenser for water removal. The gas mixture is then sent to the second detector (PDHID) in the GC and left gases were vented. An explanation for the two detectors can be seen in the GC section (see p21). An input-output diagram of the BESR system is shown in Figure 2.3.4.

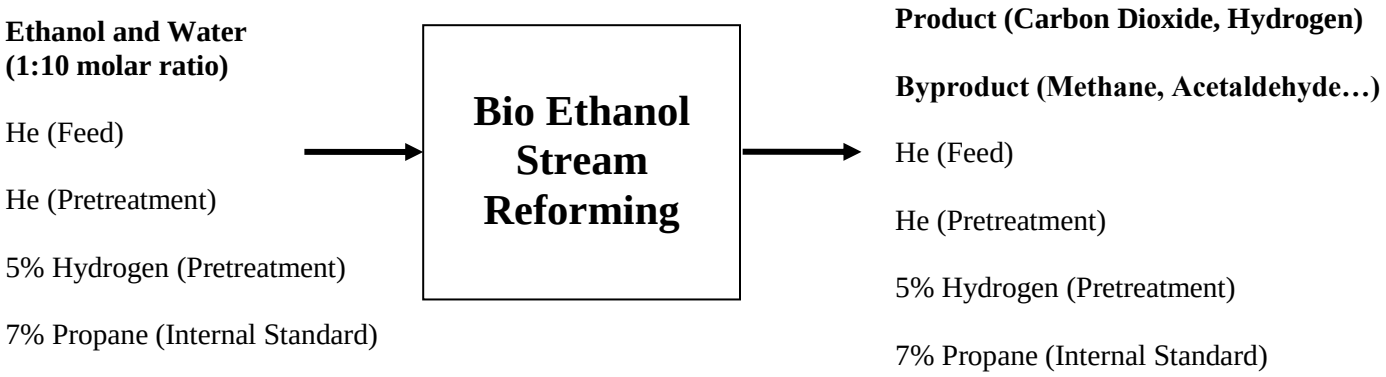

Figure 2.3.4 Input-Output Diagram of the BESR System

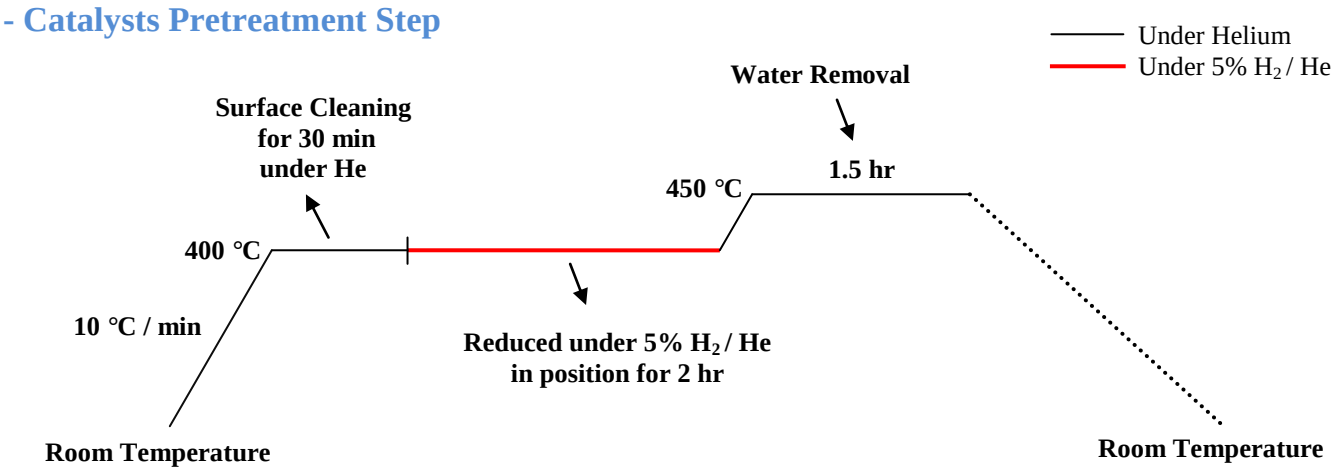

Figure 2.3.5 Catalysts Pretreatment Process

All catalysts were pretreated before reaction. The catalysts were first pretreated for the purpose of surface cleaning at 400 ℃ for 30 minutes under helium. The catalysts were then reduced under 5% hydrogen and helium for 2 hours at the same temperature and remained for 1.5 hours at 450 ℃ under He to remove the water.

- BESR Reaction

After pretreatment, the catalyst activity test was conducted in the temperature range of 350 ℃ to 500 ℃. As the temperature was increased by 50℃, the reaction products and byproducts were identified at each temperature by the gas chromatography. The catalyst held at each temperature for 2 hours and two samples are analyzed with the GC which are collected at the end of each hour, the results are then averaged for each temperature step. The catalytic performance tests were carried out for all 10% weight loading Co/CeO_2 nanocrystals. The hydrogen yield, carbon containing product yield, selectivity and ethanol conversion were calculated at different temperatures.

- Reactor

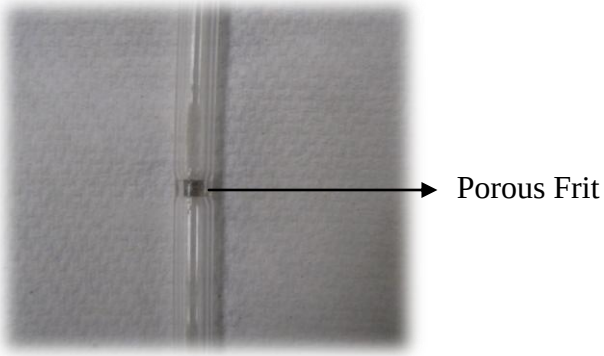

Figure 2.3.6 4mm ID Quartz Reactor

30 mg of 10% Co/CeO_2 catalysts were loaded in a 4mm in inner diameter quartz reactor with a fixed porous frit. The porous frit is used to hold the catalysts in the reactor and does not have an effect on the catalytic activity.

B. Gas Chromatography (GC)

Gas chromatography is one of the most commonly used analytical instrument to separate a gas mixture based on their volatilities. Gas Chromatography is also capable of identifying each compound of that mixture through separation and subsequent detection process by providing quantitative information such as concentrations of the compound. The Gas Chromatography can be divided by three major components: The injection section, the GC column section and the detector section. If the mixture is not in gaseous state, the injector of the GC is set up at high temperature in order to volatize the mixture [29]. The carrier gas (mobile phase) such as helium then flows through the gas mixture and transfers to the GC column which is covered by the liquid phase (stationary phase) [30]. As the gas mixture and the mobile phase travels along with the column, each compound moves at different velocity due to divergent interactions with the stationary phase. The velocity difference results in various arrival times at the detector which is called the "retention time". When the detector perceives the compound, it generates electricity signal and this appears as spectral peaks in the screen. The size of those peaks is called "Response Factor".

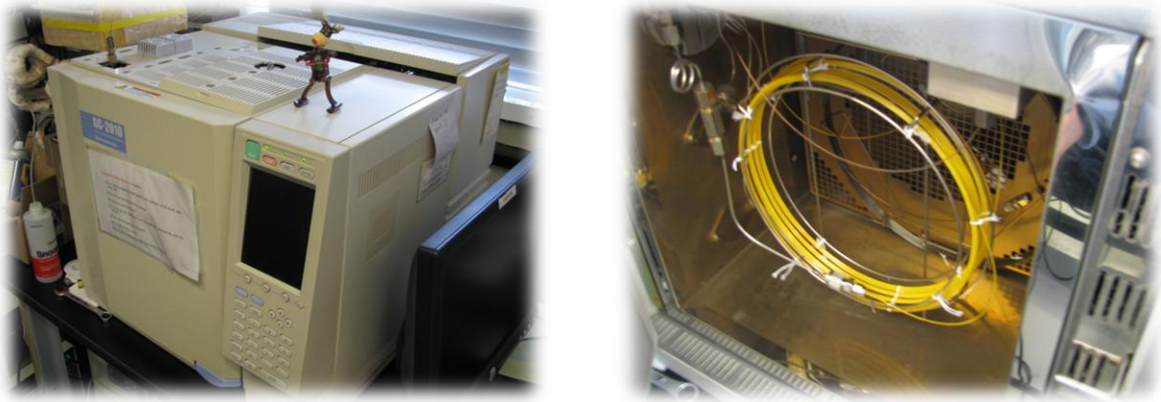

Figure 2.3.7 Gas Chromatography and Columns (Shimadzu Scientific 2010)

The response factor varies with the amount of the materials that reaches to the detector, thus by calibrating the GC in terms of concentration; the calibrated response factors can be conjugated to resolve the concentrations of unknown materials. Therefore, the GC that was used in the experiment was calibrated for all the reaction related compounds in the range of expected concentrations. The retention time of reactants and possible reaction products for BESR are shown in Table 2.3.1.

Table 2.3.1 GC Retention Time for All Reaction Products

PDHID	**Retention Time (s)**
Hydrogen	1.8
Carbon Monoxide	2.7
Carbon Dioxide	10.9
Propane	38
FID	**Retention Time (s)**
Methane	9.6
Ethane	12
Propane	14.5
Acetaldehyde	15.5
Ethanol	19
Acetone	22

In the experiment, a specialized gas chromatograph (Shimadzu Scientific 2010) was used to estimate the activity of the catalysts, and the reaction related compounds were detected. Two detectors were used for analysis. The detectors are called as 'Pulse Discharge Helium Ionization Detector (PDHID)' and 'Flame Ionization Detector (FID). The PDHID was used to detect the major products such as hydrogen and carbon dioxide, and FID was used to detect most of the organic compounds.

C. Definition of Yield, Selectivity and Conversion

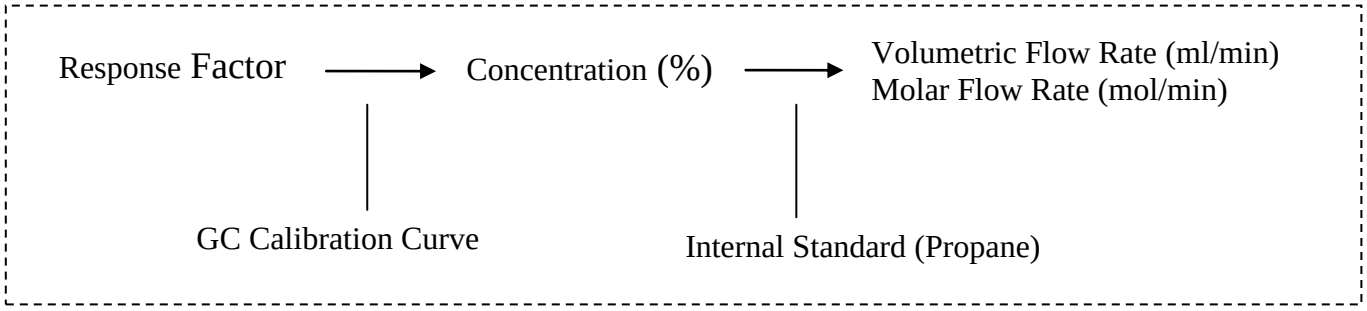

Figure 2.3.8 Procedures for Molar Flow Rate Calculation

To determine the numbers of moles of every reactants and reaction products, first the response factor of those substances were converted to concentration using the GC calibration curve. An internal standard (7% propane) was then used to calculate the volumetric flow rate and molar flow rate from the concentration. Detailed internal standard calculations are shown in Appendix B as example. The hydrogen yield, selectivity and yield of carbon containing product, and ethanol conversion were defined as the following equations. The number of moles that were used for these equations were based on 1min.

- Hydrogen Yield

$$Hydrogen\ Yield\ \% = \frac{Moles\ of\ Hydrogen\ Produced}{6\ \times Moles\ of\ Ethanol\ Fed} \times 100 \qquad [2.3.1]$$

- Yield of Carbon containing Product

$$Carbon\ Containing\ Product\ Yield\ \% = \frac{Numbers\ of\ Carbon\ in\ Product\ \times Moles\ of\ Product}{2\ \times Moles\ of\ Ethanol\ Fed} \times 100 \qquad [2.3.2]$$

- Selectivity of Carbon containing Product

$$Carbon\ Containing\ Product\ Selectivity\ \% = \frac{Numbers\ of\ Carbon\ in\ Product\ \times Moles\ of\ Product}{2\ \times Moles\ of\ Ethanol\ Converted} \times 100 \qquad [2.3.3]$$

- Ethanol Conversion

$$Ethanol\ Conversion\ \% = \frac{Moles\ of\ Ethanol\ Converted}{Moles\ of\ Ethanol\ Fed} \times 100 \qquad [2.3.4]$$

3. Results and Discussion

3.1 TEM Images for CeO_2 morphologies

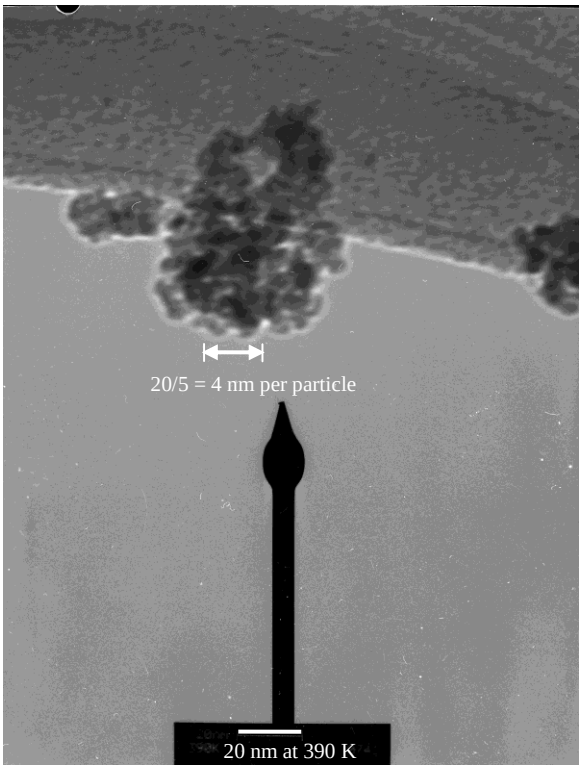

Figure 3.1.1 TEM images of CeO_2 Nanopolyhedra (*Taken by Ibrahim Ilgaz Soykal)*

All TEM images are taken by a PhD student, Ibrahim Ilgaz Soykal. The TEM image of CeO_2 nanopolyhedra were approximately 4-8 nm per particle in length. The nanopolyhedra were shaped similar to spherical, and existed in aggregate state. Figure 3.1.1 indicates that the size of nanopolyhedra is quite uniformed. The obtained CeO_2 nanopolyhedra are relatively small compared to other nanoparticles synthesized in the project. It has been reported that the size of nanopolyhedra fairly rely on the reaction temperature [25]. Therefore, it is expected by increasing the reaction temperature larger CeO_2 nanopolyhedra can be observed which explains the larger particle sizes achieved by the nanocubes in Figure 3.1.2.

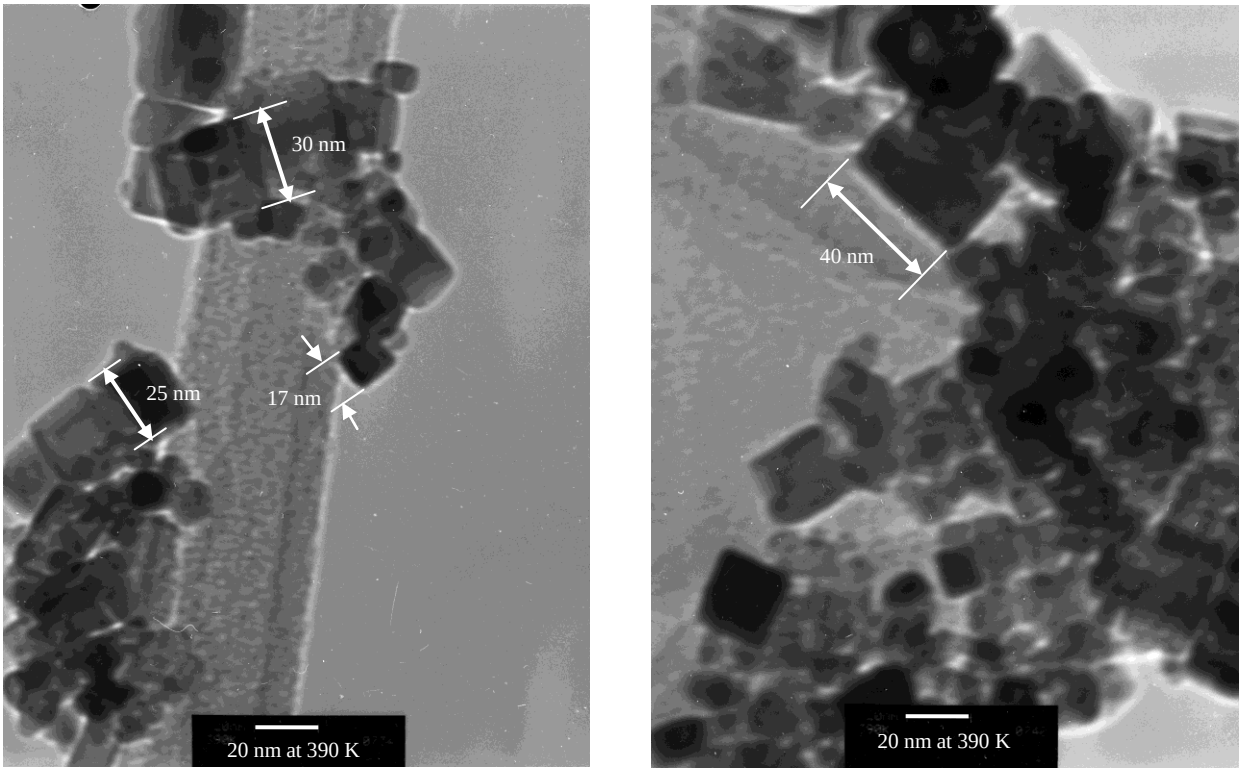

Figure 3.1.2 TEM images of CeO_2 Nanocubes (*Taken by Ibrahim Ilgaz Soykal)*

CeO_2 nanocubes are shown in Figure 3.1.2. The size of nanocubes were varied from 17nm up to 40nm in length. However, imprecise shapes of nanocubes that are smaller than 17nm can also be found in this figure, and most of them are adhered to the large size of nanocubes. Since the CeO_2 nanopolyhedra represent the most fundamental nanocrystal structure for all morphologies and the crystal growth of nanopolyhedra play a pivotal role on producing CeO_2 nanocubes and nanorods, these round shape and small size morphologies can be inferred as nanopolyhedra that were in the progression of crystal growth. Therefore these nanopolyhedra that coexist with nanocubes, corroborates the fact that CeO_2 nanopolyhedra are the source of re-crystallization for nanocubes.

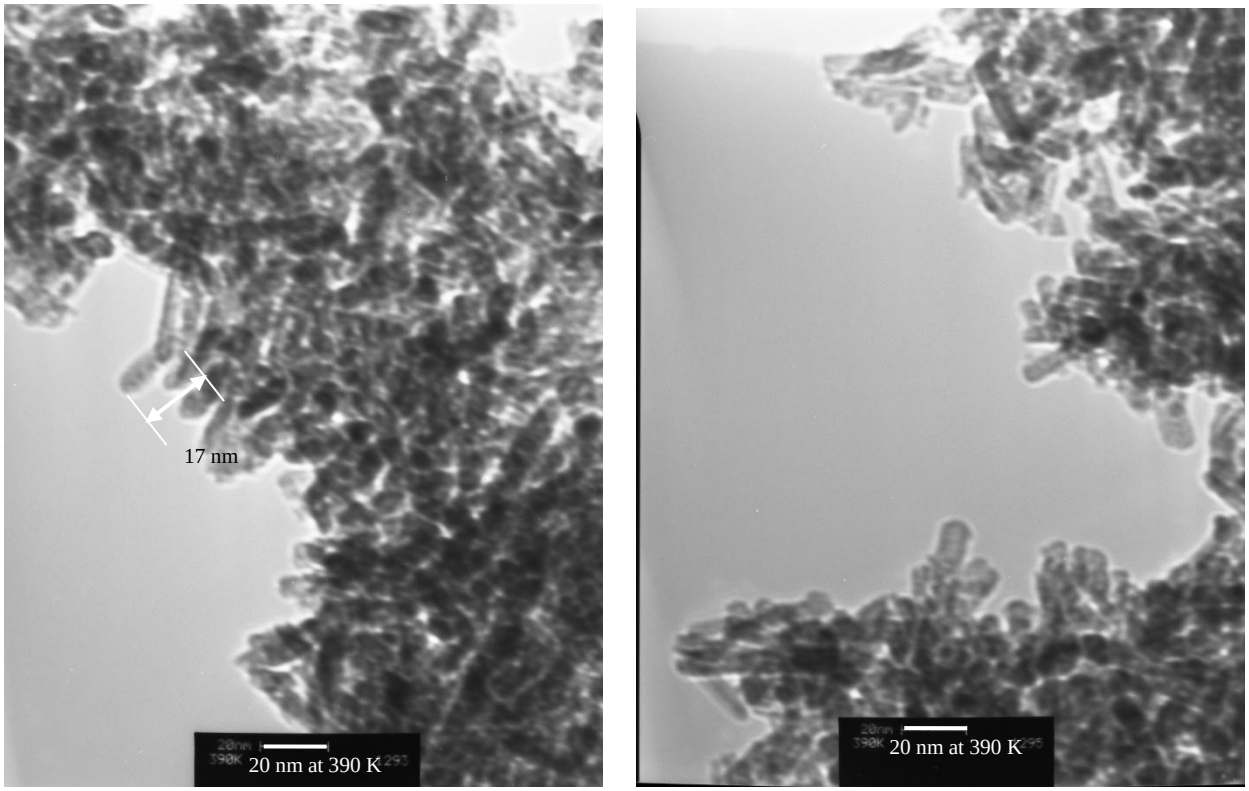

Figure 3.1.3 TEM images of CeO_2 Nanorods (*Taken by Ibrahim Ilgaz Soykal)*

The crystal structure of CeO_2 nanorods are displayed distinctly in Figure 3.1.3. The TEM result shows that the nanorods subsists in cohesion state similar to nanopolyhedra. The nanorods were shown in the size range 15-20 nm. As naonocubes are not present in the figure, this fact indicates that the reaction temperature for nanorods was precisely controlled. From the result, it would be recommended to initiate a research in regard to the determination for transition temperature between nanorods and nanocubes.

All of the TEM images substantiates that the preparation procedures were exact to fabricate CeO_2 morphologies. The reaction temperature was appropriate for the crystal growth of nanopolyhedra to nanorods and cubes. Unfortunately, the images do not show the crystal lattice in detail, therefore there is a room for improvement in TEM images.

3.2 BET Results

Table 3.2.1 BET Surface Area and Pore Volume

	BET Surface Area (m^2/g)	Pore Volume (cm^3/g)
CeO_2 Nanopolyhedra	100	0.17
CeO_2 Nanorods	**100**	**0.39**
CeO_2 Nanocubes	**60**	**0.12**
Co/CeO_2 Nanopolyhedra	56	0.12
Co/CeO_2 Nanorods	**87**	**0.35**
Co/CeO_2 Nanocubes	**40**	**0.09**

The BET results are tabulated in Table 3.2.1. When comparing all the data for CeO_2 supports, the BET surface area of nanopolyhedra and nanorods were 100 m^2/g and nanocubes showed the least value of 60 m^2/g. There was a same trend in the pore volume part, however in here nanorods had the highest pore volume of 0.39 cm^3/g. After cobalt impregnation, both BET surface area and the pore volume of all Co/CeO_2 catalysts were decreased. The most likely possible explanation for this is that cobalt molecules may cover the porosities of the support and diminish the surface area. Comparing the BET surface area of Co/CeO_2 catalysts, the highest value was 87 m^2/g for nanorods, and it also had the highest pore volume of 0.35 cm^3/g. When putting all the data together, nanorods appears to have the highest BET surface area and pore volume of both CeO_2 and Co/CeO_2, and nanocubes contains the least BET surface area and pore volume of both CeO_2 and Co/CeO_2.

The influence of BET surface area and pore volume on the activity of the Co/CeO_2 catalysts cannot be well defined. That is because there are always various characteristics of a certain catalyst that should be taken into consideration when the performance is determined as a whole. The result of BET surface area and pore volume will be discussed again later after catalytic activity results are presented.

3.3 BESR Reaction Results

A. Gas Chromatography Calibration Results

The first GC calibration was conducted on February, 2011. When the response factors for each substance were graphed as a function of concentration, a linear trend line was added by setting the intercept at zero in order to determine the best fit line for the data. These calibration curves and linear equations can be seen in Appendix C. However, there were some deviated data points from the linear trend line especially for carbon monoxide and carbon dioxide, also more data points were essential to draw an accurate calibration curve which may have a potential to occur errors in the catalytic activity test. Therefore, the GC was calibrated again on March, 2011. This time a second degree polynomial equation was applied for the data, and more data points were collected. Table 3.3.1 includes the coefficients for this second degree polynomial equation $y = Ax^2 + Bx$ that was practically used to obtain the concentration of each reaction product.

Table 3.3.1 Coefficients for the Calibration Curve

	Detector	A	B
Hydrogen (H_2)	PDHID	0	$1.74e^{-07}$
Methane (CH_4)	FID	0	$4.02e^{-07}$
Ethane (C_2H_5)	FID	0	$2.68e^{-07}$
Acetaldehyde (CH_3CHO)	FID	0	$1.33e^{-06}$
Carbon Monoxide (CO)	PDHID	$1.84e^{-16}$	$1.29e^{-07}$
Carbon Dioxide (CO_2)	PDHID	$1.79e^{-14}$	$3.81e^{-08}$
Propane (C_3H_7)	PDHID	0	$1.23e^{-07}$
Propane (C_3H_7)	FID	0	$1.90e^{-07}$
Acetone $(CH_3)_2CO$	FID	0	$4.48e^{-07}$
Ethanol (C_2H_5OH)	FID	0	$4.50e^{-07}$

B. Catalytic Activity Results for Co/CeO_2 Morphologies

After the catalytic activity tests were finished, hydrogen yield, selectivity and yield of carbon containing product, and ethanol conversion were calculated for all CeO_2 support morphologies in each temperature. These values can be seen in Table 3.3.2 through 3.3.4. Reaction product data in terms of concentrations, volumetric flow rates, and molar flow rates are located in Appendix D. A detailed comparative analysis of conversion and yield was performed for all support morphologies. Since the carbon containing product selectivity shows a similar trend to its yield, only the reaction products that have a selectivity of higher than 10% was graphed (acetaldehyde, carbon dioxide). The sum of all selectivity does not equal to 100 %. This is because other byproducts were generated during the reaction which was not either detected or unidentified. However, the carbon balances were shown over 90% in the experiment.

Table 3.3.2 Data Analysis Results for Co/CeO_2 Nanopolyhedra (%)

	Hydrogen Yield	**Ethanol Conversion**	**Methane Yield**	**Ethane Yield**	**Acetaldehyde Yield**	**Acetone Yield**	**CO Yield**	**CO2 Yield**
350 °C	65.8	80.8	1.47	0.08	2.84	1.91	-	71.8
400 °C	87.6	93.5	1.24	0.08	-	1.93	-	81.5
450 °C	91.1	100	1.24	0.13	-	-	-	89.7
500 °C	90.6	100	0.98	-	-	-	-	90.9
	Methane Selectivity	**Ethane Selectivity**	**Acetaldehyde Selectivity**	**Acetone Selectivity**	**CO Selectivity**	**CO2 Selectivity**		
350 °C	1.82	0.09	3.52	2.37	-	88.8		
400 °C	1.33	0.08	-	2.07	-	87.1		
450 °C	1.24	0.13	-	-	-	89.7		
500 °C	0.98	-	-	-	-	90.9		

Table 3.3.3 Data Analysis Results for Co/CeO_2 Nanorods (%)

	Hydrogen Yield	Ethanol Conversion	Methane Yield	Ethane Yield	Acetaldehyde Yield	Acetone Yield	CO Yield	CO2 Yield
350 ℃	18.9	75.7	1.44	0.07	44.9	12.3	-	4.02
400 ℃	33.4	78.5	1.98	0.32	28.8	14.9	-	18.6
450 ℃	50.5	81.8	2.02	1.13	15.1	-	-	35.8
500 ℃	90.9	100	3.39	-	-	-	-	87.3
	Methane Selectivity	**Ethane Selectivity**	**Acetaldehyde Selectivity**	**Acetone Selectivity**	**CO Selectivity**	**CO2 Selectivity**		
350 ℃	1.90	0.09	59.3	16.3	-	5.31		
400 ℃	2.53	0.41	36.7	19.1	-	23.7		
450 ℃	2.47	1.38	18.5	-	-	43.8		
500 ℃	3.39	-	-	-	-	87.3		

Table 3.3.4 Data Analysis Results for Co/CeO_2 Nanocubes (%)

	Hydrogen Yield	Ethanol Conversion	Methane Yield	Ethane Yield	Acetaldehyde Yield	Acetone Yield	CO Yield	CO2 Yield
350 ℃	53.1	60.4	1.59	0.11	9.84	4.97	-	41.0
400 ℃	84.9	85.7	1.51	0.47	1.48	8.03	-	70.3
450 ℃	96.1	100	1.71	0.17	-	-	-	90.0
500 ℃	96.1	100	1.44	-	-	-	-	92.7
	Methane Selectivity	**Ethane Selectivity**	**Acetaldehyde Selectivity**	**Acetone Selectivity**	**CO Selectivity**	**CO2 Selectivity**		
350 ℃	2.64	0.18	16.3	8.23	-	67.9		
400 ℃	1.76	0.55	1.73	9.38	-	82.1		
450 ℃	1.71	0.17	-	-	-	90.0		
500 ℃	1.44	-	-	-	-	92.7		

- Discussion

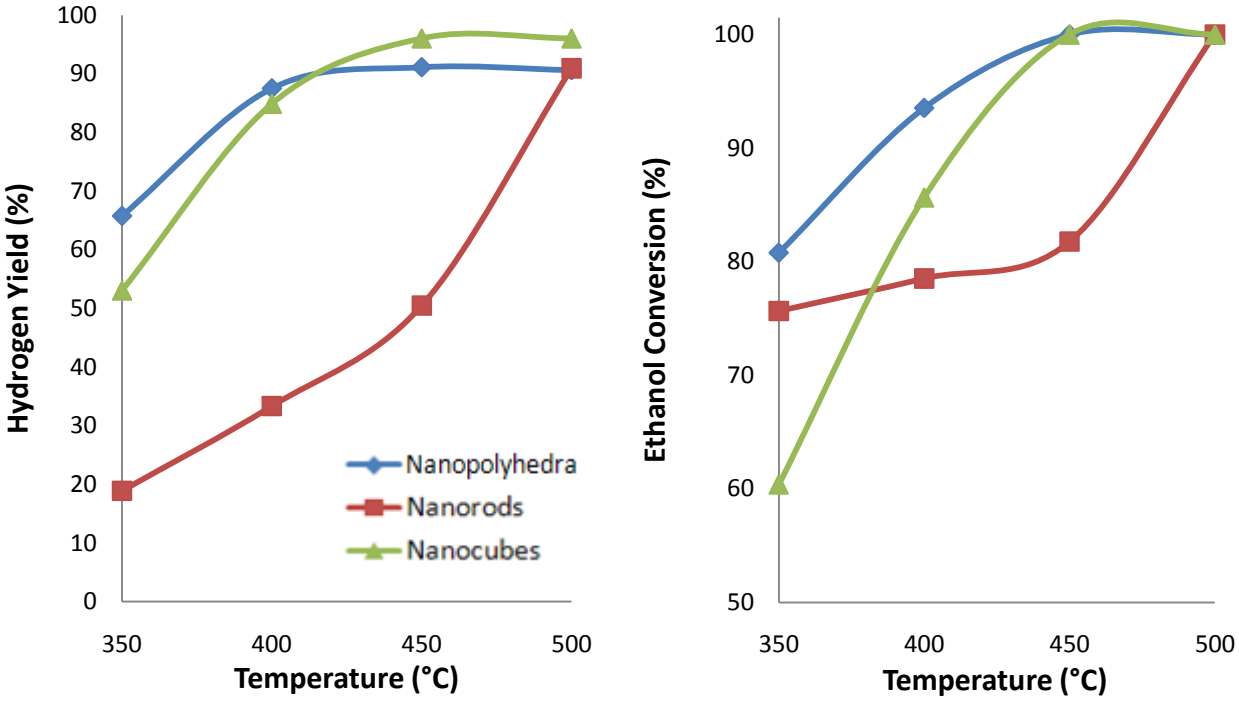

Figure 3.3.1 Activity Results for Hydrogen Yield and Ethanol Conversion

Figure 3.3.1 shows a trend that both hydrogen yield and ethanol conversion increase as the temperature increases. However, when the temperature reaches at 450 ℃, those values for Co/CeO_2 nanopolyhedra and cubes remain roughly constant, whereas Co/CeO_2 nanorods show a rapid increase. These results show that 450 ℃ can be determined as the optimal temperature for Co/CeO_2 nanopolyhedra and cubes in BESR. The Co/CeO_2 nanopolyhedra show a better catalytic activity results than other morphologies at low temperature. At 350 ℃ the hydrogen yield is obtained as high as 66% over Co/CeO_2 nanopolyhedra, and as low as 19% over Co/CeO_2 nanorods. However, the ethanol conversion for Co/CeO_2 nanorods at 350 ℃ is much higher than nanocubes. This can be due to side reactions that occur during the reaction. In other words, other products such as methane, acetone and acetaldehyde are quite dominant for Co/CeO_2 nanorods

than other morphologies. At 500 ℃, the hydrogen yield of 96 % over Co/CeO_2 nanocubes is achieved as the highest value. For nanorods, the hydrogen yield of 91% and ethanol conversion of 100% are shown as maximum values at 500℃. Therefore, 500 ℃ can be the optimal temperature for Co/CeO_2 nanorods in BESR.

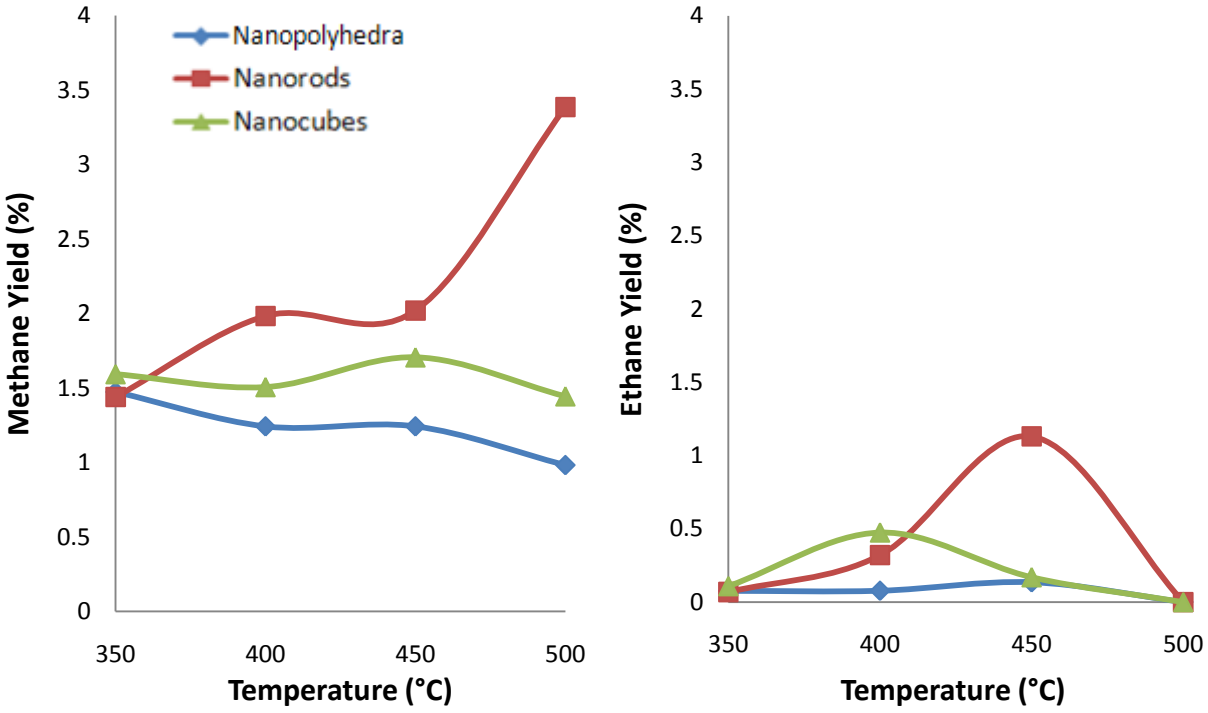

Figure 3.3.2 Activity Results for Methane and Ethane Yield

As it is expected, the methane and ethane yields over Co/CeO_2 nanorods are mostly higher than nanopolyhedra and nanobcubes since nanorods show lower hydrogen yields for all temperatures. Methane can be produced by either ethanol decomposition or methanation (see p2) and the formation is limited to temperature in the range of 300 ℃ to 400 ℃. Thus, the descending methane yield curves for Co/CeO_2 nanopolyhedra and cubes are graphed appropriately after 450 ℃. However, the ascending curve for Co/CeO_2 nanorods shows an

abnormal trend. A possible explanation for this is that the ethanol decomposition becomes dominant after temperature of 450 ℃ for Co/CeO_2 nanorods. This result corresponds to the rapid increase of hydrogen yield over Co/CeO_2 nanorods after 450 ℃ since hydrogen can be also produced by ethanol decomposition.

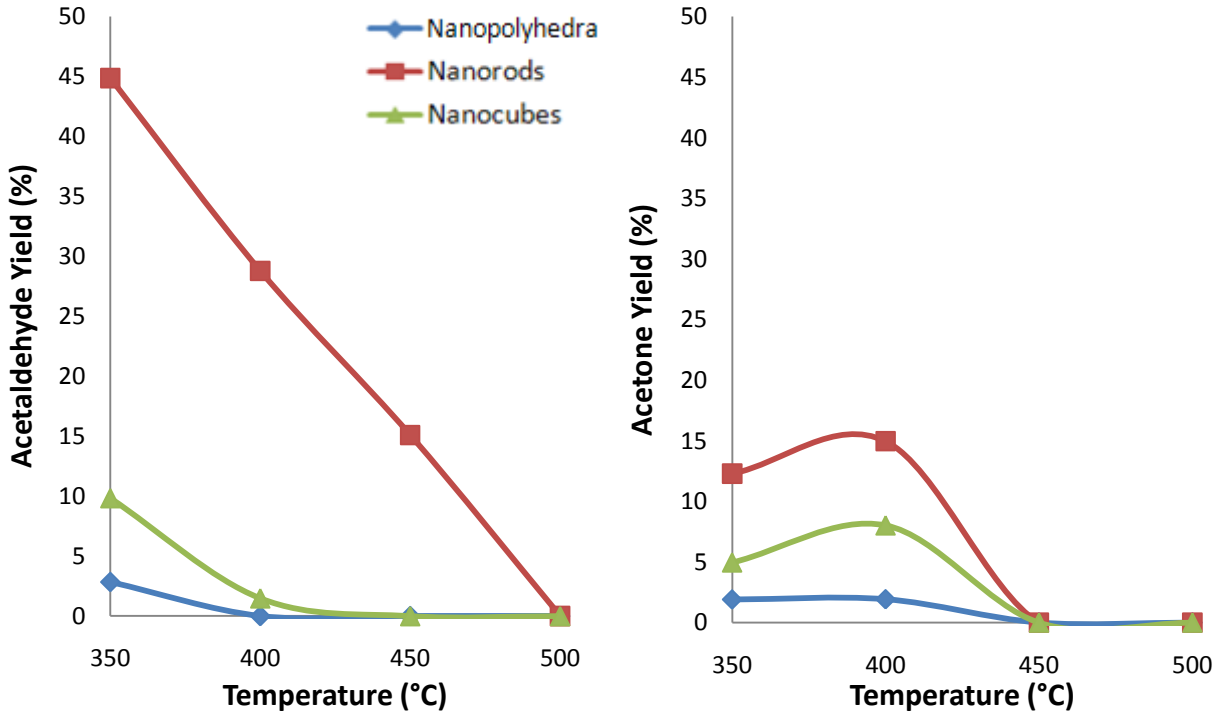

Figure 3.3.3 Activity Results for Acetaldehyde and Acetone Yield

Acetaldehyde and acetone yield decreases as temperature increases for all Co/CeO_2 morphologies. At 350 ℃, almost 45% of acetaldehyde was produced from using Co/CeO_2 nanorods and only 3% of acetaldehyde and acetone was produced over Co/CeO_2 nanopolyhedra . The correlation between morphologies seen here also corresponds to the hydrogen yield curve; in other words, low acetaldehyde yield have a potential to give high hydrogen yields. At 500 ℃

acetaldehyde and acetone production was not observed for all morphologies. This is because it was such a small amount which was below the GC's sensitivity.

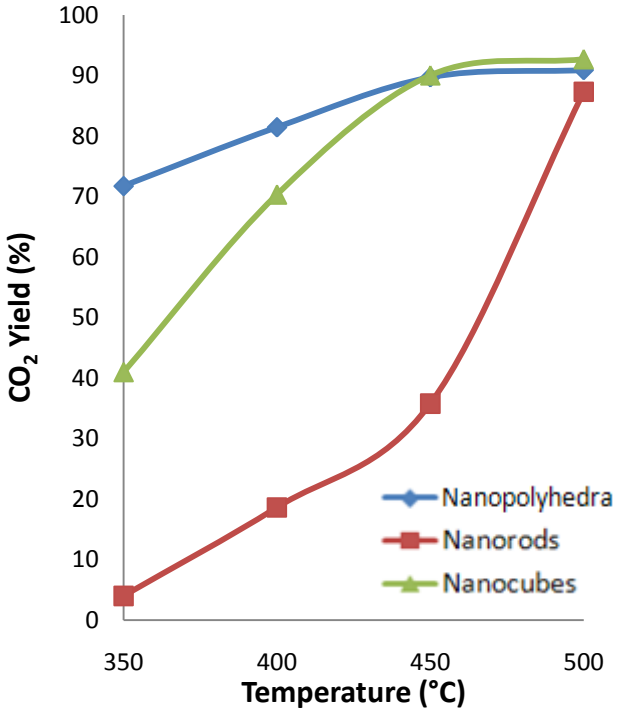

Figure 3.3.4 Activity Results for CO_2 Yield

Carbon dioxide is one of the major products, and is an important factor when looking into the performance of a specific catalyst for BESR. If carbon dioxide is produced nearly to the theoretical prediction which shows 100% yield, the catalyst can be considered as active because this means that only the main reaction has been taken place. If the carbon dioxide yield is much smaller than theoretical yield, this indicates that side reactions have happened. This becomes clearer when the selectivity results are taken into account simultaneously with the results of byproducts yield. In Figure 3.3.4, a small quantity of CO_2 yield of 4% is presented initially over Co/CeO_2 nanorods whereas nanopolyhedra show 72% which is almost 18 times higher. This

result indicates that the Co/CeO_2 nanopolyhedra are more active than other morphologies at low temperature which is very similar to the findings from hydrogen yield and ethanol conversion graphs. On the other hand, at high temperature such as 450 ℃ to 500 ℃, the carbon dioxide yield for Co/CeO_2 nanocubes overcomes the value of nanopolyhedra. Therefore, Co/CeO_2 nanocubes are found to become more active than nanopolyhedra at high temperature.

Throughout the reaction, carbon monoxide was not detected by the GC or its concentration was insignificant. The selectivity that is depicted in Figure 3.3.5 follows the same trend in carbon containing product yield graphs. The rapid descending acetaldehyde selectivity curve and the ascending carbon dioxide selectivity curve against temperature for Co/CeO_2 nanorods can be seen in here as well.

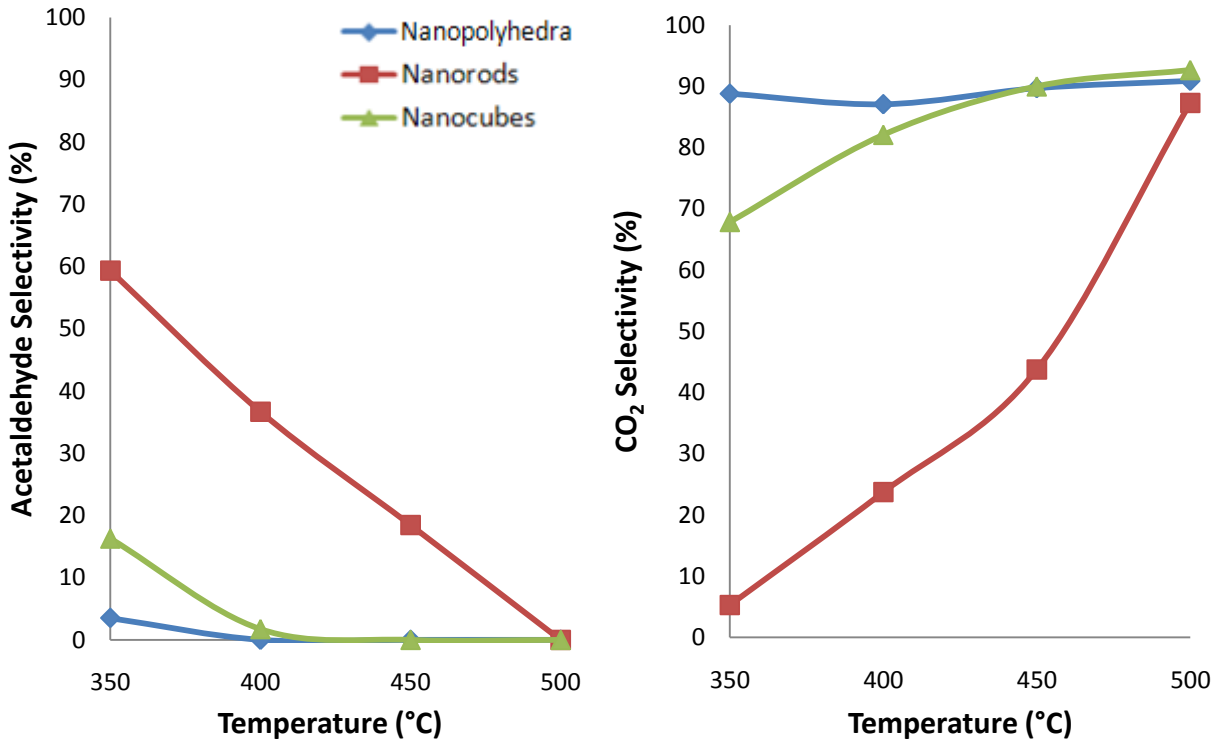

Figure 3.3.5 Activity Results for Acetaldehyde and CO_2 Selectivity

4. Conclusion and Recommendations

In this paper, cerium oxide as a catalysts support was synthesized with different morphologies such as nanopolyhedra, nanorods, nanocubes under specific conditions. The present TEM results show that cerium oxide nanopolyhedra in agglomeration state are 4-8 nm per particle in diameter revealing nearly spherical shape. Nanorods are shown in the size range of 15-20 nm and nanocubes dimensions are diverse from 17nm up to 40nm in length. Therefore, these TEM images confirmed that nanocrystal morphologies were clearly synthesized under proper temperature and pressure. After the supports morphologies were synthesized, cobalt precursor was impregnated to have a cobalt loading of 10 wt. % by incipient wetness impregnation (IWI) method.

BET Characterization results showed that both CeO_2 and Co/CeO_2 nanorods exhibited the largest BET surface area and pore volume, whereas nanocubes showed the smallest. Higher surface area and pore volume were expected to play a role in improving hydrogen production. However, from the activity tests results, Co/CeO_2 nanocubes showed the best catalytic performance at high temperature (450, 500 ℃), showing the highest hydrogen yield of 96 % and 100% ethanol conversion at 500 ℃. Also, Co/CeO_2 nanopolyhedra were the most activated catalysts at low temperature (350, 400 ℃), indicating the highest hydrogen yield of 87.5% and 93.5% ethanol conversion at 400 ℃. Therefore, it is concluded that other effective factors would improve the catalytic performance of Co/CeO_2 with different morphologies. To better understand how support morphology affects on the catalytic performance of Co/CeO_2 on ethanol steam reforming, more characterization Diffuse Reflectance Infrared Fourier Transform Spectroscopy (DRIFTS) and X-ray diffraction (XRD) can be carried out. Also, applying higher temperature such as 550-650 ℃ and different amount of cobalt loading can be worth for further studies.

5. References

1. Kalinci, Y., A. Hepbasli, and I. Dincer, *Biomass-based hydrogen production: A review and analysis.* International Journal of Hydrogen Energy, 2009. **34**(21): p. 8799-8817.
2. Song, H., et al., *Investigation of bio-ethanol steam reforming over cobalt-based catalysts.* Catalysis Today, 2007. **129**(3-4): p. 346-354.
3. Aupretre, F., C. Descorme, and D. Duprez, *Hydrogen Production for Fuel Cells from the Catalytic Ethanol Steam Reforming.* Topics in Catalysis, 2004. **30**: p. 487-491.
4. Benito, M., et al., *Bio-ethanol steam reforming: Insights on the mechanism for hydrogen production.* Journal of Power Sources, 2005. **151**: p. 11-17.
5. Song, H. and U.S. Ozkan, *Economic analysis of hydrogen production through a bio-ethanol steam reforming process: Sensitivity analyses and cost estimations.* International Journal of Hydrogen Energy, 2010. **35**(1): p. 127-134.
6. Song, H., B. Mirkelamoglu, and U.S. Ozkan, *Effect of cobalt precursor on the performance of ceria-supported cobalt catalysts for ethanol steam reforming.* Applied Catalysis a-General, 2010. **382**(1): p. 58-64.
7. Palo, D.R., R.A. Dagle, and J.D. Holladay, *Methanol steam reforming for hydrogen production.* Chemical Reviews, 2007. **107**(10): p. 3992-4021.
8. Bshish, A., et al., *Steam-reforming of ethanol for hydrogen production.* Chemical Papers, 2011. **65**(3): p. 251-266.
9. Feng, D., et al., *Steam reforming of dimethyl ether over CuO-ZnO-Al_2O_3-ZrO_2+ZSM-5: A kinetic study.* Chemical Engineering Journal, 2009. **146**(3): p. 477-485.
10. Comas, J., et al., *Methane steam reforming and ethanol steam reforming using a Ni(II)-Al(III) catalyst prepared from lamellar double hydroxides.* Chemical Engineering Journal, 2006. **118**(1-2): p. 11-15.
11. Biswas, P. and D. Kunzru, *Steam reforming of ethanol for production of hydrogen over Ni/CeO_2–ZrO_2 catalyst: Effect of support and metal loading.* International Journal of Hydrogen Energy, 2007. **32**(8): p. 969-980.
12. Kadam, K.L. and J.D. McMillan, *Availability of corn stover as a sustainable feedstock for bioethanol production.* Bioresource Technology, 2003. **88**(1): p. 17-25.
13. Lin, S.S.Y., D.H. Kim, and S.Y. Ha, *Metallic phases of cobalt-based catalysts in ethanol steam reforming: The effect of cerium oxide.* Applied Catalysis A, General, 2009. **355**(1-2): p. 69-77.
14. Aupretre, F., C. Descorme, and D. Duprez, *Bio-ethanol catalytic steam reforming over supported metal catalysts.* Catalysis Communications, 2002. **3**(6): p. 263-267.
15. Llorca, J., et al., *Efficient Production of Hydrogen over Supported Cobalt Catalysts from Ethanol Steam Reforming.* Journal of Catalysis, 2002. **209**(2): p. 306-317.
16. Batista, M.S., et al., *Characterization of the activity and stability of supported cobalt catalysts for the steam reforming of ethanol.* Journal of Power Sources, 2003. **124**(1): p. 99-103.
17. Haga, F., et al., *Catalytic properties of supported cobalt catalysts for steam reforming of ethanol.* Catalysis Letters, 1997. **48**(3-4): p. 223-227.
18. Song, H. and U.S. Ozkan, *Ethanol steam reforming over Co-based catalysts: Role of oxygen mobility.* Journal of Catalysis, 2009. **261**(1): p. 66-74.

19. Wang, H., et al., *Study on the carbon deposition in steam reforming of ethanol over Co/CeO_2 catalyst.* Chemical Engineering Journal, 2008. **145**(1): p. 25-31.
20. Song, H., B. Tan, and U.S. Ozkan, *Novel Synthesis Techniques for Preparation of Co/CeO_2 as Ethanol Steam Reforming Catalysts.* Catalysis Letters, 2009. **132**(3-4): p. 422-429.
21. Song, H. and U.S. Ozkan, *The role of impregnation medium on the activity of ceria-supported cobalt catalysts for ethanol steam reforming.* Journal of Molecular Catalysis A-Chemical, 2010. **318**(1-2): p. 21-29.
22. Hsiao, W.-I., et al., *The effect of the morphology of nanocrystalline CeO_2 on ethanol reforming.* Chemical Physics Letters, 2007. **441**(4-6): p. 294-299.
23. Zhou, K., et al., *Enhanced catalytic activity of ceria nanorods from well-defined reactive crystal planes.* Journal of Catalysis, 2005. **229**(1): p. 206-212.
24. Byrappa, K. and M. Yoshimura, *Handbook of Hydrothermal Technology - A Technology for Crystal Growth and Materials Processing*. 2001, William Andrew Publishing/Noyes.
25. Shih, C.J., Y.J. Chen, and M.H. Hon, *Synthesis and crystal kinetics of cerium oxide nanocrystallites prepared by co-precipitation process.* Materials Chemistry and Physics, 2010. **121**(1-2): p. 99-102.
26. "CM-200." *The Campus Electron Optics Facility*. The Ohio State University. Web. 12 July 2011. <http://www.ceof.ohio-state.edu/Instruments/CM200.html>.
27. "The Transmission Electron Microscope." *Nobelprize.org*. Nobel Media AB 2011. Web. 08 July 2011. <http://nobelprize.org/educational/physics/microscopes/tem/index.html>.
28. Brunauer S, Emmett PH, Teller E. Adsorption of gases in multimolecular layers. *J Am Chem Soc.* 1938;60:309–319. doi: 10.1021/ja01269a023.
29. "Gas Chromatography." *UC Boulder Organic Chemistry Undergraduate Courses*. University of Colorado, Boulder, Chemistry and Biochemistry Department, 2011. Web. 12 July 2011. <http://orgchem.colorado.edu/hndbksupport/GC/GC.html>.
30. "Gas Chromatography Theory." *UCLA Chemistry and Biochemistry*. 10 Aug. 2006. Web. 12 July 2011. <http://www.chem.ucla.edu/~bacher/General/30BL/gc/theory.html>.

Appendix A. Calculations for Volumetric Flow Rate of the Pump

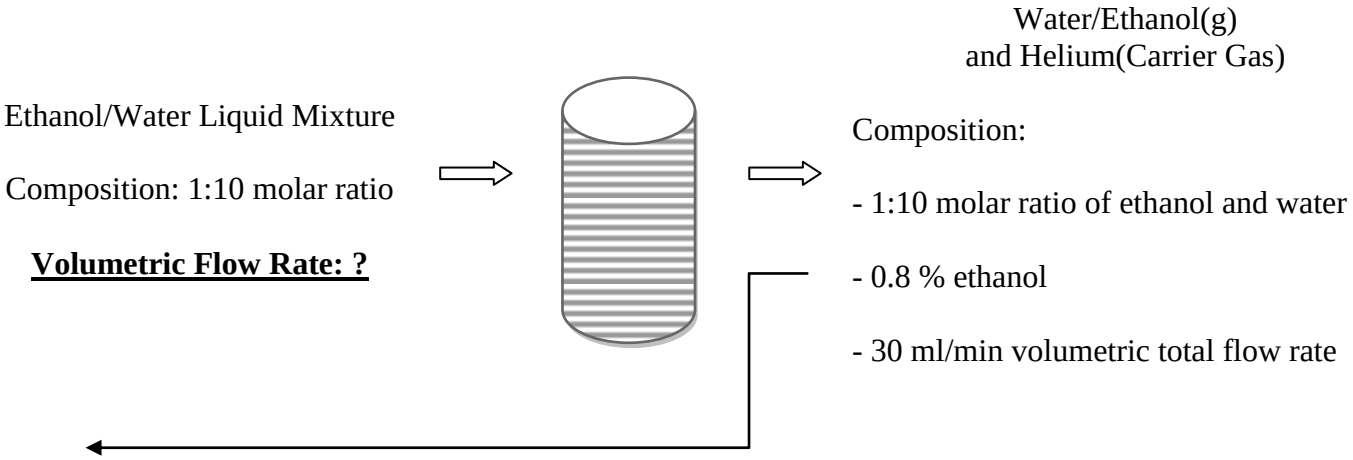

From the ideal gas law, at same pressure and temperature, the 1:10 molar ratio is convertible to 1:10 concentration ratio. Therefore, in total flow rate of 30ml/min

$$Total\ Flow\ Rate = 30\,\frac{ml}{min}$$

$$0.8\,\%\ Ethanol = 0.24\,\frac{ml}{min} \qquad 8\,\%\ Water = 2.4\,\frac{ml}{min} \qquad 91.2\,\%\ Helium = 27.36\,\frac{ml}{min}$$

Using Ideal Gas Law:

$$PV = nRT \qquad n = \frac{PV}{RT} \qquad \dot{N} = \frac{P\dot{V}}{RT}$$

Therefore,

$$\dot{N} = \frac{\boldsymbol{P} \times \dot{\boldsymbol{V}}}{\boldsymbol{R} \times \boldsymbol{T}}$$

$$\dot{N} = Molar\ Flow\ Rate\ (\frac{mol}{min})$$

$$\dot{V} = Volumetric\ Flow\ Rate\ (\frac{ml}{min})$$

$$P = 1\ atm \quad T = 298\ K\ (Room\ Temperature)$$

$$R\ (Gas\ Constant) = 8.205746\ \times\ 10^{-5}\ (\frac{m^3 \cdot atm}{K \cdot mol})$$

$$\dot{N}_{Ethanol} = \frac{1\ atm\ \times\ 0.24\frac{ml}{min}\ \times\ 10^{-6}\ \frac{m^3}{ml}}{8.205746\ \times\ 10^{-5}\ \left(\frac{m^3 \cdot atm}{K \cdot mol}\right) \times\ 298\ K} = 0.000009814\ \frac{mol}{min}$$

$$\dot{N}_{Water} = \frac{1\ atm\ \times\ 0.24\frac{ml}{min}\ \times\ 10^{-6}\ \frac{m^3}{ml}}{8.205746\ \times\ 10^{-5}\ (\frac{m^3 \cdot atm}{K \cdot mol})\ \times\ 298\ K} = 0.00009815\ \frac{mol}{min}$$

Density of Ethanol: $0.789\frac{g}{cm^3}$ Density of Water (Liquid): $1\frac{g}{cm^3}$

Molecular Weight of Ethanol: $46\ \frac{g}{mol}$ Molecular Weight of Water (Liquid): $18\frac{g}{mol}$

$$Ethanol\ Flow\ Rate = \ 0.000009814\ \frac{mol}{min}\ \times\ 46\ \frac{g}{mol}\ \times \frac{1}{0.789\frac{g}{cm^3}} = 0.000572\ \frac{ml}{min}$$

$$Water\ Flow\ Rate = \ 0.00009815\ \frac{mol}{min}\ \times\ 18\ \frac{g}{mol}\ \times \frac{1}{1\frac{g}{cm^3}} = 0.0017667\ \frac{ml}{min}$$

$$Total\ \ Volumetric\ Flow\ Rate = 0.000572 + 0.0017667 = 0.0023387\ \frac{ml}{min} = \ 0.1403\ \frac{ml}{hr}$$

Therefore, the pump volumetric flow rate was determined as $\mathbf{0.1403}\ \frac{\boldsymbol{ml}}{\boldsymbol{hr}}$

Appendix B. Internal Standard Calculation for GC

The total volumetric flow rate of 35 ml/min after reactor (feed + propane) cannot be used to calculate the molar flow rate (mol/min) of each substance in the GC. That is because the total volumetric flow rate (ml/min) of the feed may increase during the reaction. Therefore, 7% propane of 5 ml/min which was controlled was employed as the internal standard to derive the total volume flow rate. This part involves the sequence of calculation of the molar flow rate for each substance, and hydrogen was used as an example.

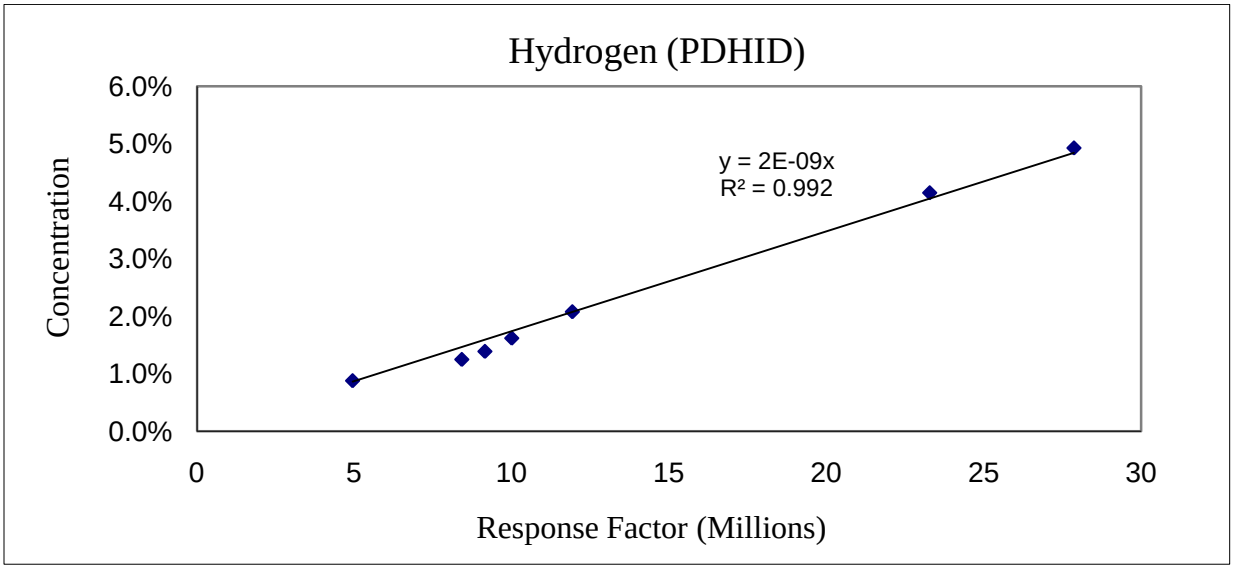

Figure 1. GC Calibration Curve of Hydrogen (PDHID): This figure shows the trend-line for the GC calibration data of hydrogen. The data was collected on February 2010.

Step 1: Concentration (%)

Assuming that 15 million response factor was obtained from the GC by integrating the hydrogen peaks, the concentration of hydrogen can be calculated from the calibrated graph function.

$$Y = 2 \times 10^{-0.9} \times X = 2 \times 10^{-0.9} \times 15 = \mathbf{3.77}\ \%$$

Step 2: Volumetric Flow Rate (ml/min)

Assume that propane concentration was also gained as 0.87%, according to Step 1.

$$Concentration\ of\ Hydrogen\ (C_H)\ = \frac{Volumetric\ Flow\ Rate\ of\ Hydrogen\ (\dot{V}_H)}{Total\ Volumetric\ Flow\ Rate\ (\dot{V}_T)}$$

$$Concentration\ of\ Propane\ (C_P)\ = \frac{Volumetric\ Flow\ Rate\ of\ Hydrogen\ (\dot{V}_P)}{Total\ Volumetric\ Flow\ Rate\ (\dot{V}_T)}$$

Therefore, $\dot{V}_T = \frac{\dot{V}_H}{C_H} = \frac{\dot{V}_P}{C_P}$ $\quad \boxed{\boldsymbol{\dot{V}_H = C_H \times \frac{\dot{V}_P}{C_P}}}$

The volumetric flow rate of 7% propane was set at 5 ml/min in the experiment.

$$\dot{V}_p = 5\ \frac{ml}{min} \times 0.07 = 0.35 \frac{ml}{min}$$

$$Volumetric\ Flow\ Rate\ of\ Hydrogen\ (\dot{V}_H) = 3.77\ \% \times \frac{0.35\ ml/min}{0.87\ \%} = \mathbf{1.51}\ \boldsymbol{\frac{ml}{min}}$$

Step 3: Molar Flow Rate (mol/min) – Using Ideal Gas Equation

The produced gases are assumed to follow the ideal gas law in the experiment.

Ideal Gas Law:

$$PV = nRT$$

$$n = \frac{PV}{RT} \qquad \dot{N} = \frac{P\dot{V}}{RT}$$

$$\dot{N}_H = \frac{P \times \dot{V}_H}{R \times T}\ (for\ Hydrogen)$$

Therefore,

$$\dot{N}_H = \frac{P \times \dot{V_H}}{R \times T}$$

$$\dot{N_H} = Molar\ Flow\ Rate\ of\ Hydrogen\ (\frac{mol}{min})$$

$$\dot{V_H} = Volumetric\ Flow\ Rate\ of\ Hydrogen\ (\frac{ml}{min})$$

$$P = 1\ atm \quad T = 273\ K\ (0°\ C) -\ after\ condenser$$

$$R\ (Gas\ Constant) = 8.205746\ \times\ 10^{-5}\ (\frac{m^3 \cdot atm}{K \cdot mol})$$

$$\dot{N}_H\ \left(\frac{umol}{min}\right) = \frac{1\ atm \times \dot{V_H}}{8.205746 \times 10^{-5}\ \frac{m^3 \cdot atm}{K \cdot mol} \times 273\ K}\ \times \frac{1\ cm^3}{1\ ml} \times \frac{1\ m^3}{10^6\ cm^3} \times \frac{10^6\ umol}{mol}$$

$$= \dot{V_H} \times 44.63949607$$

This coefficient can be used for unit conversion in this specific BESR system.

$$\frac{ml}{min} \text{ -> } \frac{umol}{min}$$

Therefore,

$$\dot{N_P} = Molar\ Flow\ Rate\ of\ Propane = 0.350\ \frac{ml}{min} \times 44.63949607\ = \mathbf{15.62}\ \frac{\boldsymbol{umol}}{\boldsymbol{min}}$$

$$\dot{N_H} = Molar\ Flow\ Rate\ of\ Hydrogen = 1.51\ \frac{ml}{min} \times 44.63949607\ = \mathbf{67.41}\ \frac{\boldsymbol{umol}}{\boldsymbol{min}}$$

Step 3: Molar Flow Rate (mol/min) – Using Propane Gas

The produced gases are assumed to follow the ideal gas law in the experiment.

Avogadro's Law

$$\frac{P_1 \times V_1}{T_1 \times N_1} = \frac{P_2 \times V_2}{P_2 \times N_2}$$

At same pressure and temperature,

$$\frac{V_1}{N_1} = \frac{V_2}{N_2} \quad or \quad N_1 = \frac{V_1 \times N_2}{V_2}$$

Therefore,

$$\boldsymbol{\dot{N}_H = \frac{\dot{V}_H \times \dot{N}_P}{\dot{V}_P}}$$

$\dot{N}_H = Molar\ Flow\ Rate\ of\ Hydrogen\ (\frac{mol}{min})$

$\dot{N}_P = Molar\ Flow\ Rate\ of\ Propane\ (\frac{mol}{min})$

$\dot{V}_H = Volumetric\ Flow\ Rate\ of\ Hydrogen\ (\frac{ml}{min})$

$\dot{V}_P = Volumetric\ Flow\ Rate\ of\ Hydrogen\ (\frac{ml}{min})$

$$\dot{N}_P = \dot{V}_P \left(\frac{ml}{s}\right) \times \rho \left(\frac{kg}{m^3}\right) \times \frac{1}{M} \left(\frac{mol}{g}\right) \times \frac{1}{1000000} \frac{m^3}{cm^3} \times \frac{1000\ g}{kg}$$

$$\rho \left(\frac{kg}{m^3}\right) = density\ of\ propane\ (gas) = 2\ \frac{kg}{m^3}$$

$$M \left(\frac{mol}{gmol}\right) = Molecular\ Weight\ of\ propane = 44 \frac{g}{mol}$$

$$\dot{N}_H = \frac{\dot{V}_H \times \cancel{\dot{V}_P} \times 2 \times \frac{1}{44} \times \frac{1}{1000000} \times 1000}{\cancel{\dot{V}_P}} = \dot{V}_H \times 2 \times \frac{1}{44} \times \frac{1}{1000000} \times 1000$$

$$= \dot{V}_H \times \frac{1}{22} \times \frac{1}{1000} \left(\frac{mol}{min}\right)$$

Unit Change to umol/min

$$\dot{N}_H = \dot{V}_H \times \frac{1}{22} \times \frac{1}{10^3} \frac{mol}{min} \times 10^6 \frac{umol}{mol} = \boxed{\dot{\boldsymbol{V}}_{\boldsymbol{H}} \times \frac{\mathbf{1}}{\mathbf{22}} \times \mathbf{10^3}}$$

Therefore,

$$\dot{N}_p = Molar\ Flow\ Rate\ of\ Propane = 0.350 \frac{ml}{min} \times \frac{1}{22} \times 10^3 \frac{umol}{min} = \mathbf{15.91}\ \frac{\boldsymbol{umol}}{\boldsymbol{min}}$$

$$\dot{N}_H = Molar\ Flow\ Rate\ of\ Hydrogen = 1.51 \frac{ml}{min} \times \frac{1}{22} \times 10^3 \frac{umol}{min} = \mathbf{68.63}\ \frac{\boldsymbol{umol}}{\boldsymbol{min}}$$

Appendix C. GC Calibration Graphs (February 2010)

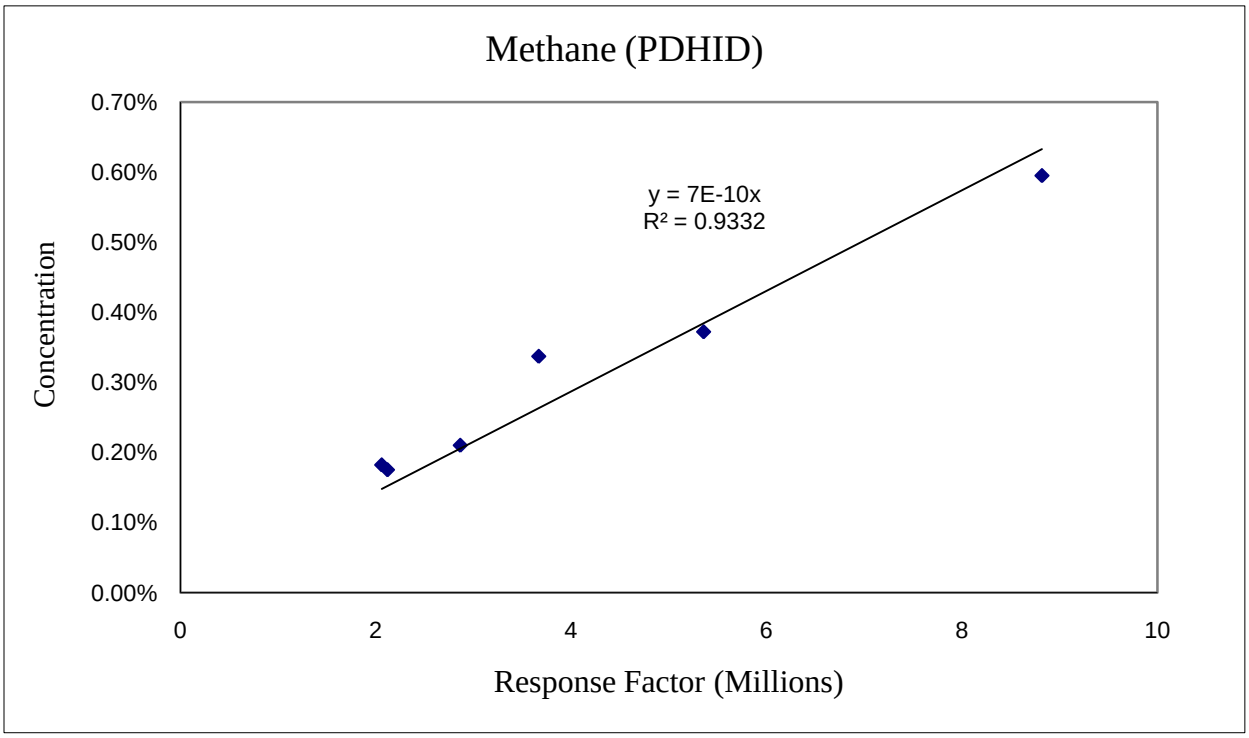

Figure 2. GC Calibration Curve of Methane (PDHID)

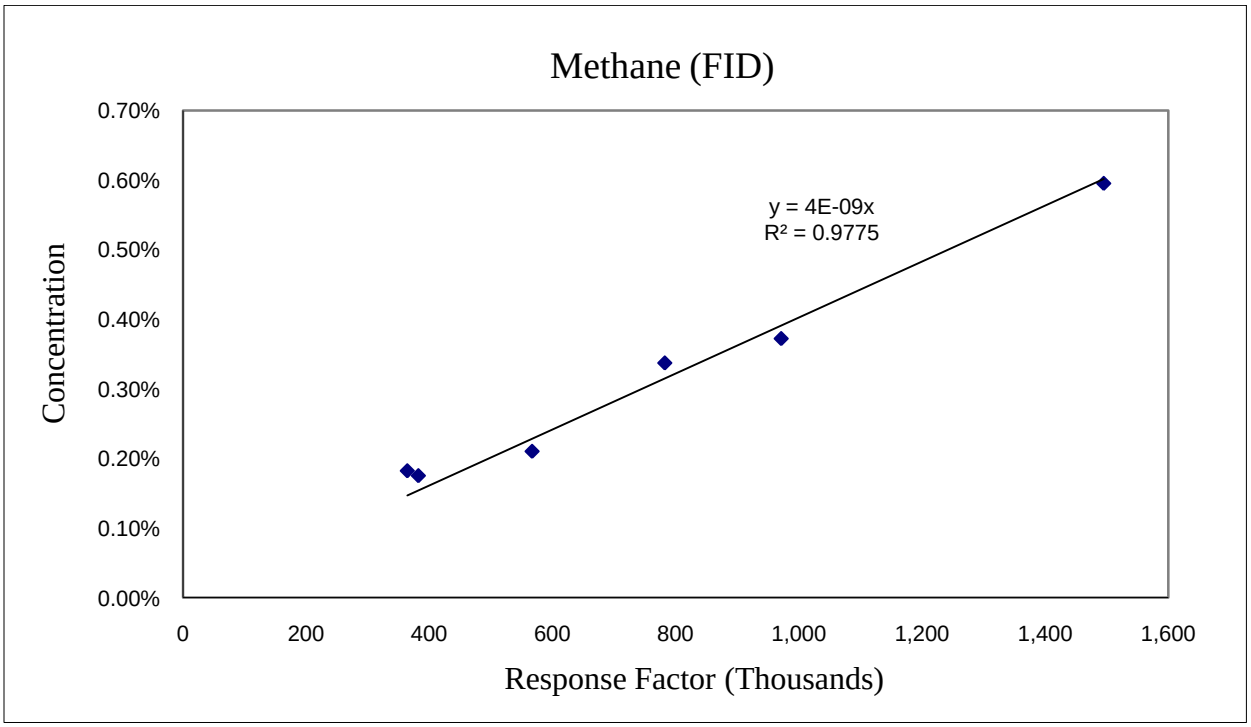

Figure 3. GC Calibration Curve of Methane (FID)

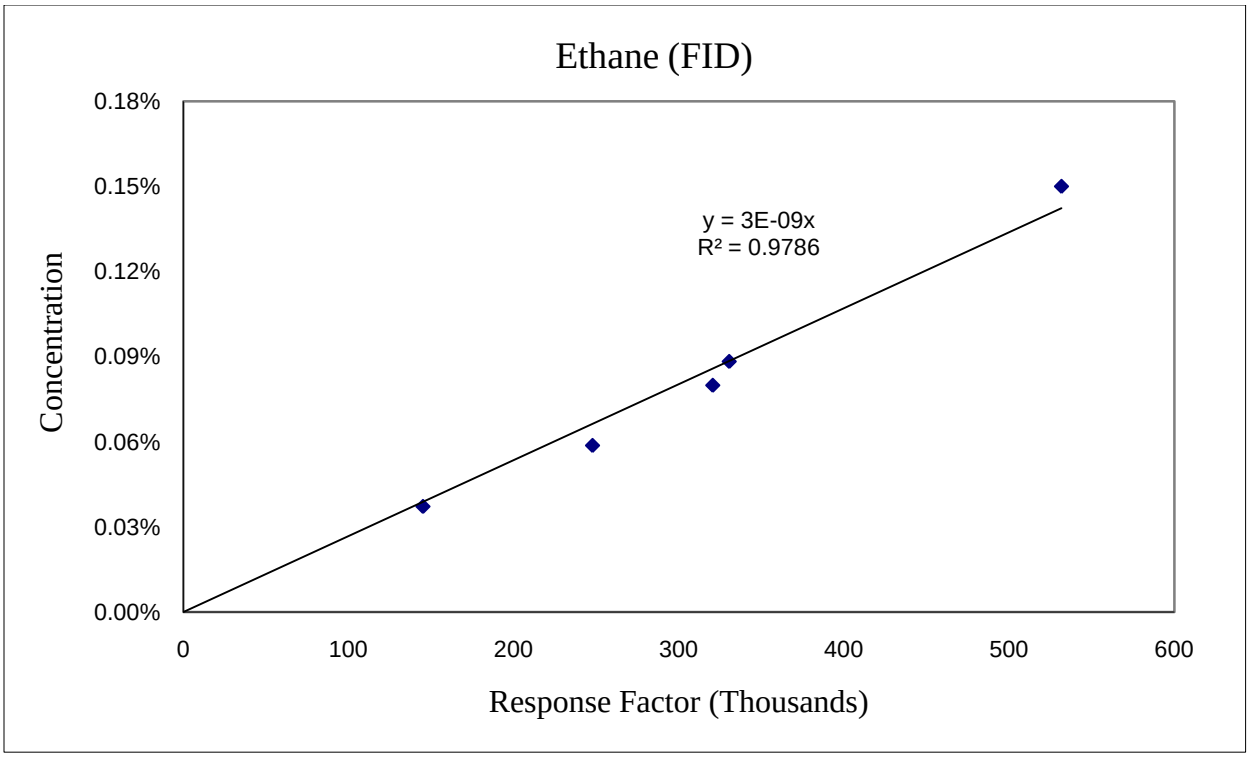

Figure 4. GC Calibration Curve of Ethane (FID)

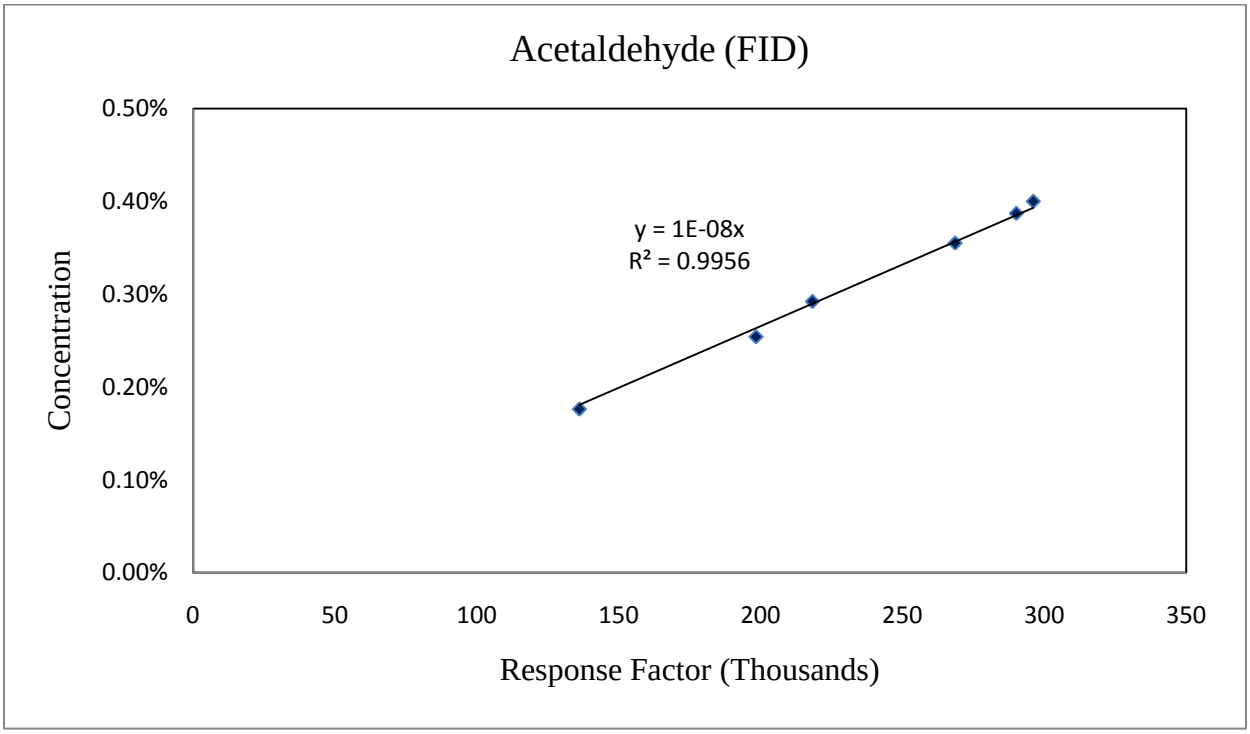

Figure 5. GC Calibration Curve of Acetaldehyde (FID)

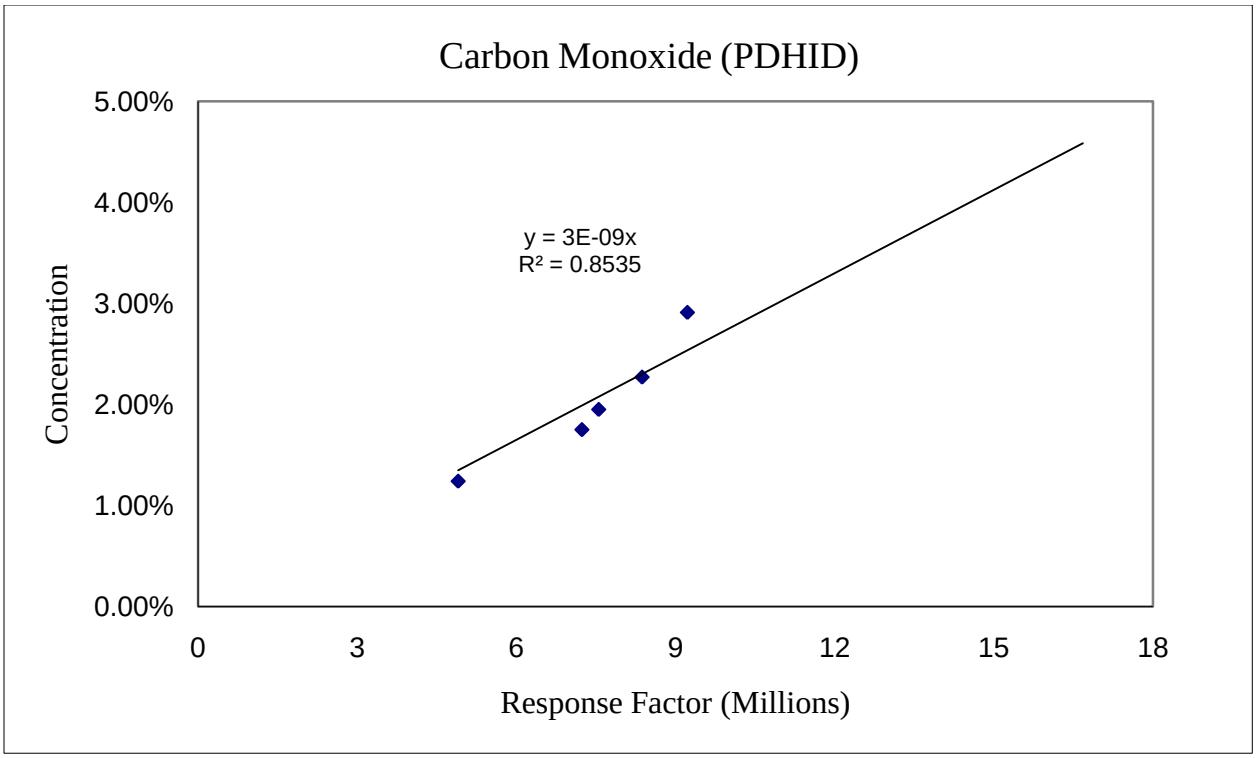

Figure 6. GC Calibration Curve of Carbon Monoxide (PDHID)

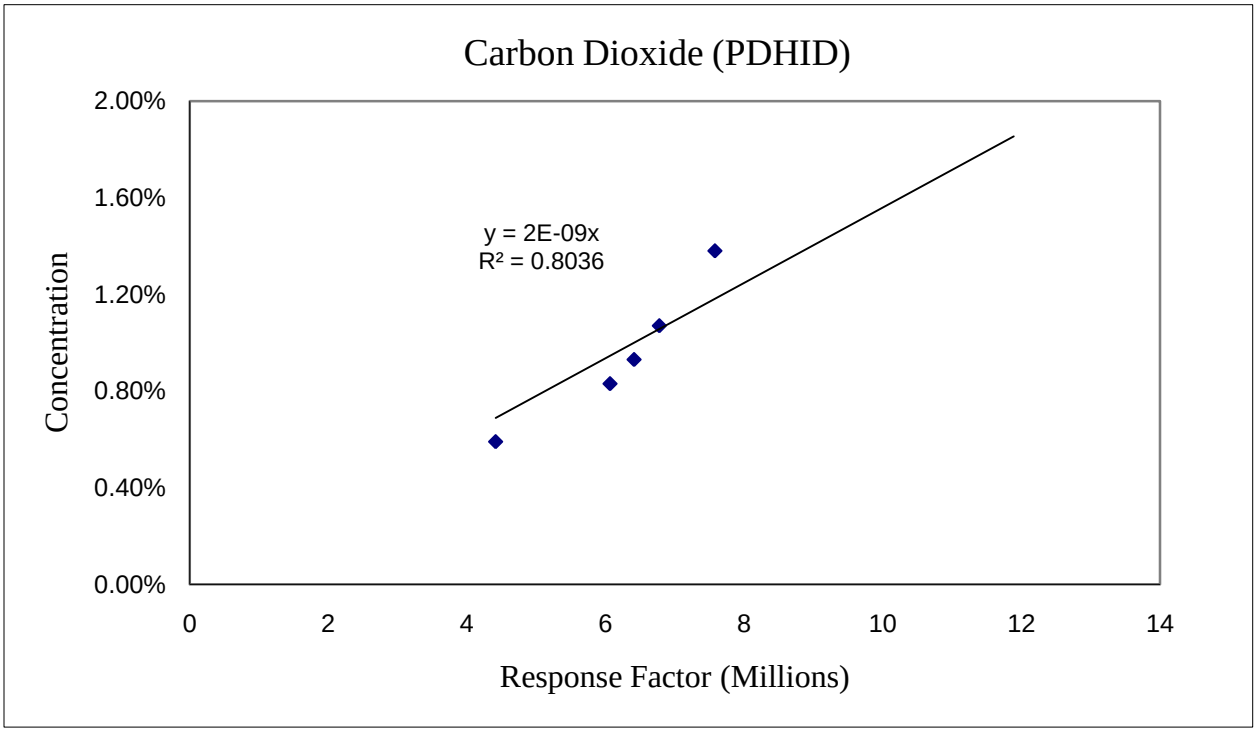

Figure 7. GC Calibration Curve of Carbon Dioxide (PDHID)

Appendix D. Reaction Product Data

Table 1. Reaction Product Data for Co/CeO_2 Nanopolyhedra

Concentrations (%)	**Hydrogen**	**Ethanol**	**Methane**	**Ethane**	**Acetaldehyde**	**Acetone**	**CO**	**CO2**	**Propane**
Feed	-	0.73	-	-	-	0.06	-	-	1.04
350 ℃	2.40	0.14	0.02	-	0.02	0.01	-	0.87	1.00
400 ℃	3.15	0.05	0.02	-	-	0.01	-	0.98	0.99
450 ℃	3.18	-	0.02	-	-	-	-	1.04	0.99
500 ℃	3.17	-	0.01	-	-	-	-	1.06	0.99
Flow Rate (ml/min)									
Feed	-	0.25	-	-	-	0.02	-	-	0.35
350 ℃	0.97	0.05	0.01	-	0.01	-	-	0.35	0.35
400 ℃	1.29	0.02	0.01	-	-	-	-	0.40	0.35
450 ℃	1.35	-	0.01	-	-	-	-	0.44	0.35
500 ℃	1.34	-	-	-	-	-	-	0.45	0.35
Molar Flow Rate (umol/min)									
Feed	-	11.0	-	-	-	0.91	-	-	15.6
350 ℃	43.4	2.11	0.32	0.01	0.31	0.14	-	15.8	15.6
400 ℃	57.8	0.71	0.27	0.01	-	0.14	-	17.9	15.6
450 ℃	60.2	-	0.27	0.01	-	-	-	19.8	15.6
500 ℃	59.8	-	0.22	-	-	-	-	20.0	15.6

Table 2. Reaction Product Data for Co/CeO_2 Nanorods

Concentrations (%)	**Hydrogen**	**Ethanol**	**Methane**	**Ethane**	**Acetaldehyde**	**Acetone**	**CO**	**CO2**	**Propane**
Feed	-	0.68	-	-	-	-	-	-	1.10
350 ℃	0.59	0.15	0.02	-	0.28	0.05	-	0.04	1.03
400 ℃	1.04	0.14	0.02	-	0.18	0.06	-	0.19	1.03
450 ℃	1.63	0.11	0.02	0.01	0.09	-	-	0.38	1.01
500 ℃	2.89	-	0.04	-	-	-	-	0.92	0.97
Flow Rate (ml/min)									
Feed	-	0.21	-	-	-	-	-	-	0.35
350 ℃	0.24	0.05	0.01	-	0.10	0.02	-	0.02	0.35
400 ℃	0.43	0.05	0.01	-	0.06	0.02	-	0.08	0.35
450 ℃	0.65	0.04	0.01	-	0.03	-	-	0.15	0.35
500 ℃	1.17	-	0.01	-	-	-	-	0.37	0.35
Molar Flow Rate (umol/min)									
Feed	-	9.57	-	-	-	-	-	-	15.6
350 ℃	10.9	2.33	0.28	0.01	4.29	0.78	-	0.77	15.6
400 ℃	19.2	2.06	0.38	0.03	2.75	0.96	-	3.57	15.6
450 ℃	29.0	1.75	0.39	0.11	1.44	-	-	6.85	15.6
500 ℃	52.2	-	0.65	-	-	-	-	16.7	15.6

Table 3. Reaction Product Data for Co/CeO_2 Nanocubes

Concentrations (%)	**Hydrogen**	**Ethanol**	**Methane**	**Ethane**	**Acetaldehyde**	**Acetone**	**CO**	**CO2**	**Propane**
Feed	-	0.56	-	-	-	-	-	-	0.99
350 ℃	1.57	0.23	0.02	-	0.06	0.02	-	0.40	1.00
400 ℃	2.47	0.09	0.02	-	0.01	0.03	-	0.68	1.10
450 ℃	2.71	-	0.02	-	-	-	--	0.85	0.97
500 ℃	2.71	-	0.02	-	-	-	-	0.87	0.95
Flow Rate (ml/min)									
Feed	-	0.20	-	-	-	-	-	-	0.35
350 ℃	0.63	0.08	0.01	-	0.02	0.01	-	0.16	0.35
400 ℃	1.02	0.03	0.01	-	-	0.01	--	0.28	0.35
450 ℃	1.15	-	0.01	-	-	-	-	0.36	0.35
500 ℃	1.15	-	0.01	-	-	-	-	0.37	0.35
Molar Flow Rate (umol/min)									
Feed	-	8.90	-	-	-	-	-	-	15.6
350 ℃	28.3	3.52	0.28	0.01	0.88	0.29	-	7.29	15.6
400 ℃	45.3	1.28	0.27	0.04	0.13	0.48	-	12.5	15.6
450 ℃	51.3	-	0.30	0.02	-	-	-	16.0	15.6
500 ℃	51.3	-	0.26	-	-	-	-	16.5	15.6